ABSTRACT

ZHANG, ZHE An Application of Linear Optimization in Anaglyph Stereo Image Rendering. (Under the direction of Professor David F. McAllister).

We evaluate a new method for computing color anaglyphs based on uniform approximation in CIE color space. The method depends on the spectral distribution properties of the primaries of the monitor and the transmission functions of the filters in the viewing glasses. We will compare the result of this method with several other methods that have been proposed for computing anaglyphs. To compute the color at a given pixel in the anaglyph image requires solving a linear program. We exploit computational properties of the simplex algorithm to reduce computation time by 72 to 89 percent for the images tested. After computing the color at a pixel, a depth-first search is performed to collect all neighboring pixels with similar color so that a simple matrix-vector multiplication can be applied. We also parallelize the algorithm and implement it on a cluster environment. We discuss the effects of different data dividing schemes.

An Application of Linear Optimization in Anaglyph Stereo Image Rendering

by

Zhe Zhang

A thesis submitted to the Graduate Faculty of
North Carolina State University
in partial fulfillment of the
requirements for the Degree of
Master of Science

Operations Research

Raleigh

2006

Approved By:

Dr. S. Purushothaman Iyer	
Dr. David F. McAllister Chair of Advisory Committee	Dr. Yahya Fathi

To my mother, Xiuqing Du, and my father, Shuqing Zhang ...

Biography

Zhe Zhang is a graduate student in Operations Research and Computer Science. Born in Xi'an, Shanxi, P.R.China, he entered the University of Science and Technology of China (USTC) in September,1999 as an undergraduate student majoring in Computer Science and received his Bachelor of Engineering degree in July 2003. In August 2004 he joined the graduate program of Operations Research in the North Carolina State University (NCSU) as a Ph.D. candidate. His research interests are in stereo image rendering, distributed processing and numerical optimization.

Acknowledgements

First of all, I would like to thank Dr. David F. McAllister for being a patient supervisor and for supporting this thesis with ideas and criticism of great value. I am grateful to Dr. Yahya Fathi and Dr. S. Purushothaman Iyer for being my committee members. I want to thank Sophia Sullivan for her work on creating the image pairs and comparing the color results. I also wish to thank Eric Dubois and his student Vu Tran for the LCD anaglyph data used in this thesis. I want to thank Xiaoming Hu for his help in designing the parallel program and analyzing the results. I wish to thank Dr. Xiaosong Ma for her comments to the parallel program and the load balancing mechanism. I also want to thank Nancy McAllister for providing help in the writing of this thesis. Finally, I would like to thank Xianhua Kong whose understanding and support enabled me to finish this thesis.

Contents

List of Figures

List of Tables

Chapter 1

Introduction

We present a new method for computing color anaglyph stereo images and discuss techniques to accelerate the calculation.

Stereo computer graphics and anaglyph image rendering concepts are introduced in chapter 1. Chapter 2 discusses in detail our new uniform anaglyph calculation methods. Also included in chapter 2 is a brief introduction to linear programming concepts and techniques. In chapter 3, we present a discussion of our efforts to accelerate the uniform calculation. The results of our acceleration techniques are given in chapter 4. Chapter 5 presents our conclusions and prospective research directions.

1.1 Stereo Computer Graphics

1.1.1 Depth Cues

The human visual system uses many depth cues to disambiguate the relative positions of objects in a three-dimensional(3D) scene. These cues are divided into two categories: physiological and psychological([11]).

Physiological depth cues include the following:

Accommodation: *Accommodation* is the change in focal length of the lens of the eye as it focuses on specific regions of a 3D scene. The lens changes thickness due to

a change in tension from the ciliary muscle. This depth cue is normally used by the visual system in tandem with *convergence*.

Convergence. *Convergence*, or simply *vergence*, is the inward rotation of the eyes to converge on objects as they move closer to the observer.

Binocular disparity. *Binocular disparity* is the difference in the images projected on the left and right eye retinas in the viewing of a 3D scene. It is the salient depth cue used by the visual system to produce the sensation of depth, or *stereopsis*. Any 3D display device must be able to produce a left and right eye view and present them to the appropriate eye separately. There are many ways to do this as we will see below.

Motion parallax. *Motion parallax* provides different views of a scene in response to movement of the scene or the viewer. Consider a cloud of discrete points in space in which all points are the same color and approximately the same size. Because no other depth cues (other than binocular disparity) can be used to determine the relative depths of the points, we move our head from side to side to get several different views of the scene (called look around). We determine relative depths by noticing how much two points move relative to each other: as we move our head from left to right or up and down; the points closer to us appear to move more than points further away.

Psychological depth cues include the following:

Linear perspective. *Linear perspective* refers to the change in image size of an object on the retina in inverse proportion to the objects change in distance. Parallel lines moving away from the viewer, like the rails of a train track, converge to a vanishing point. As an object moves further away, its image becomes smaller, an effect called perspective foreshortening. This is a component of the depth cue of retinal image size.

Shading and shadowing. The amount of light from a light source illuminating a surface is inversely proportional to the square of the distance from the light source to the surface. Hence, surfaces of an object that are further from the light source are darker (shading), which gives cues of both depth and shape. Shadows cast by one object on another (shadowing) also give cues to relative position and size.

Aerial perspective. Distant objects tend to be less distinct, appearing cloudy or hazy. Blue, having a shorter wavelength, penetrates the atmosphere more easily than other colors. Hence, distant outdoor objects sometimes appear bluish. Interposition. If one object occludes, hides or overlaps (interposes) another, we assume that the object doing the hiding is closer. This is one of the most powerful depth cues.

Retinal image size. We use our knowledge of the world, linear perspective, and the relative sizes of objects to determine relative depth. If we view a picture in which an elephant is the same size as a human, we assume that the elephant is further away since we know that elephants are larger that humans.

Texture gradient. We can perceive detail more easily in objects that are closer to us. As objects become more distant, the texture becomes blurred. Texture in brick, stone, or sand, for example, is coarse in the foreground and grows finer as the distance increases.

Color. The fluids in the eye refract different wavelengths at different angles. Hence, objects of the same shape and size and at the same distance from the viewer often appear to be at different depths because of differences in color. In addition, bright-colored objects will appear to be closer than dark-colored objects.

The human visual system uses all of these depth cues to determine relative depths in a scene. In general, depth cues are additive; the more cues, the better able the viewer is to determine depth. However, binocular disparity, accommodation, and convergence are generally considered as the three most powerful cues for determining relative depth. While it is accepted by most people that binocular disparity is more important as a depth cue than accommodation and convergence, the latter two do influence depth perception when coupled with binocular disparity, especially for observer distances less than 2 meters([9]).

1.1.2 Stereoscopic Imaging

Most 3D displays fit into one or more of three broad categories: *holographic*, *multiplanar*, and *stereo pair*([11]). In general, holographic and multiplanar images produce "real" or "solid" images, in which binocular disparity, accommodation, and convergence are consistent with the apparent depth in the image.

The idea of producing stereo pair, also known as stereoscopic imaging, was first introduced by Sir Charles Wheatstone[16] in 1838. Stereo pairs simulate the binocular disparity depth cue by projecting distinct flat images to each eye. In a stereo image, since each eye is actually focused or accommodated on a flat image at a constant distance from the viewer, accommodation cues are inconsistent with the perceived depth. Consistent convergence cues are provided by the horizontal positioning of the left- and right-eye views of a scene. Binocular disparity cues are provided by computing the left- and right-eye views

from different positions relative to the scene([11]).

The computation of stereo pairs is discussed in detail in Chapter 5 of [11] and we will not cover that part here. After stereo pairs are computed, a mechanism is required in viewing them so that the left eye sees only the left eye view and the right eye sees only the right eye view([12]). It is common in display technologies to use a single screen to reflect or display both images either simultaneously (time parallel) or in sequence (time multiplexed or field sequential).

In the field-sequential or time multiplexed technique, the left/right views are alternated on the display device, and a blocking mechanism to prevent the left eye from seeing the right eye view and vice versa is required. While older technologies used mechanical devices to occlude the appropriate eye view during display refresh, newer technologies use electro-optical methods such as liquid-crystal plates. These techniques fall into two groups: those that use active vs. passive viewing glasses.

Time-parallel methods present both eye views to the viewer simultaneously and use optical techniques to direct each view to the appropriate eye. The View-Master, illustrated in Figure 1.1, is an example of time-parallel displays devices. The View-Master stereoscope uses two separate optical systems. Each eye looks though a magnifying lens to view a slide. The slides are taken with a pair of cameras mounted on a base, replicating the way we see the world with two eyes ([11]). Anaglyph, discussed in detail in section 1.2 below, is another popular time-parallel method.

1.2 Anaglyph Stereo Rendering

An anaglyph is a single image where color encoding is used to represent each of the left and right eye views, and transparent filters are placed over each eye to provide blocking. Since both images appear simultaneously, it is a time-parallel method. Each of the left and right filters has a transmission function specifying the percentages of each visible wavelength λ transmitted by the filter. A common filter standard is to divide the visible spectrum into two parts: the blue/green region at lower wavelengths and the red region at higher wavelengths. A red filter is designed to block colors with dominate wave length in the blue/green region and a blue, cyan or green filter is designed to block colors with dominate wavelengths in the red region. Examples of transmission functions for common

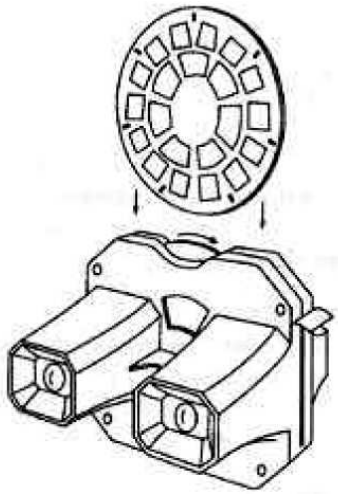

Figure 1.1: View-Master stereoscope

anaglyph filters are shown in Figure 1.2.

A significant problem of the anaglyph method is a phenomenon called *ghosting* or *cross talk*. It is caused by the fact that the filters do not completely eliminate the opposite-eye view, so that the left eye saw not only its image but sometimes part of the right-eye image as well. In this case the image can appear blurred or a second or double image appears in regions of the scene being viewed. If we observe Figure 1.2 we will find that colors with wavelengths between 550 and 600 are passed by both filters and hence ghosting will occur for colors in the region.

Another problem is that the colors seen through each filter are often not representable by the display device and hence a phenomenon called *retinal rivalry* or *binocular rivalry* will occur. Retinal rivalry refers to the fact that when the color disparity between the left- and right-eye views is very large, objects appear double, with two monocular images striking corresponding regions of the retinas. A more detailed discussion about retinal rivalry can be found in chapter 4 of [11].

Producing faithful color is also a very challenging task in anaglyph rendering. Methods like the View-Master mentioned in section 1.2 transmit each eye view separately and hence, except for possible attenuation due to the blocking mechanism, the color of the images seen by viewers is not affected. However, in the anaglyph method for every pixel the two colors, of the left- and right-eye views respectively, are encoded into a single color

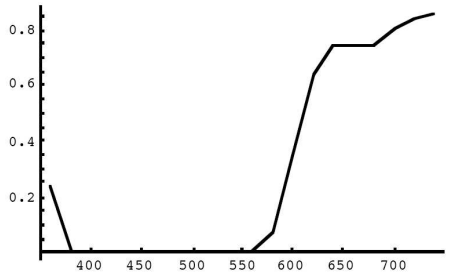

(a) Left eye transmission function - Red filter

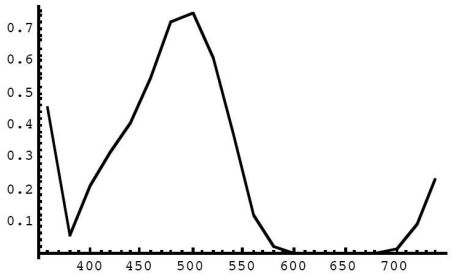

(b) Right eye transmission function - Cyan filter

Figure 1.2: Red/Cyan glasses transmission function

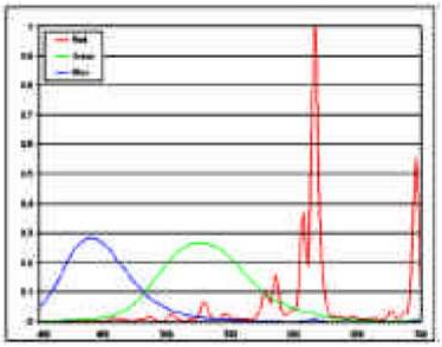

(a) CRT monitor primary distributions

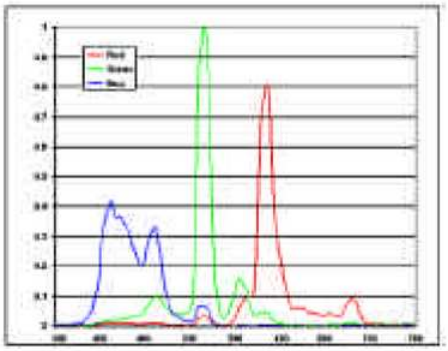

(b) LCD monitor primary distributions

Figure 1.3: Monitor spectral distributions

of the pixel in the anaglyph image. Thus it is difficult, or impossible, to represent the same amount of information contained in the two original images.

We will see in section 2.3 that all the three issues mentioned above is evident in some of the color examples, especially those produced by the existing anaglyph methods.

Because of the problems discussed above, anaglyphs have developed a bad name in the stereo community. However, the advantages of using anaglyphs vs. other methods of transmitting stereo are obvious and applications abound. For example, anaglyph can be used in virtual laboratories for distance learning applications because the stereo image can be transmitted efficiently, inexpensive viewing devices can be used and several people can view the image simultaneously([14]).

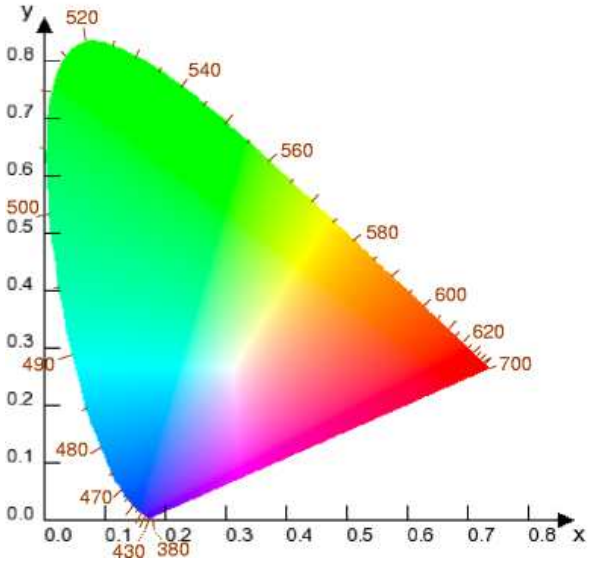

Figure 1.4: The CIE color space chromaticity diagram

1.3 Anaglyph Methods

In this section we will introduce the background(1.3.2) and several different methods(1.3.3 and 1.3.4) for producing anaglyph stereo images, which were summarized and studied by Sanders and McAllister in [14].

1.3.1 Color Spaces

Our discussion below will concern two distinct color systems. The *RGB additive color system*, which is used by most computer monitors and storage systems, produces colors by representing each of them as a linear combination of red, blue, and green.

Another color system is called the *CIE*, named after Commission Internationale de l'Eclairage, the French-language name for the International Commission on Illumination. The CIE color system characterizes colors by a luminance parameter Y and two color coordinates x and y which specify the point on the chromaticity diagram shown in Figure 1.4.

The original left- and right-eye views are represented in the RGB system. In the *least squares method* discussed in section 1.3.4 and the *uniform method* discussed in section

2 we will convert the colors into the CIE space, because the colors that can be seen through the filters, in particular those that are produced by monitors, are not representable in the RGB space, as can be observed from Figure 1.5.

1.3.2 Background of Anaglyph Calculation Methods

The set of representable colors or the color solid on a display using the RGB color system is the unit RGB cube (3- cube). The cube lies in the 3 dimensional vector space $\boldsymbol{R3}$. The basis or primaries are the colors red, green and blue.

The "anaglyph RGB color solid" in the six dimensional vector space $\boldsymbol{R6}$ is a unit hypercube (6-cube) with 64 vertices corresponding to the RGB corners of the cube in $\boldsymbol{R3}$ for the left and right eyes. Counting base 2 we can order the vertices of the 6-cube: [0,0,0,0,0,0] = [black, black], [0,0,0,0,0,1] = [black, blue],..., [1,1,1,1,1,1] = [white, white]. Anaglyph methods compute a map from the 6-cube in $\boldsymbol{R6}$ to $\boldsymbol{R3}$. We can examine the order and placement of the image of the 6- cube vertices to gain understanding of the method.

Three of the algorithms we analyze are linear; there is a 3×6 matrix representation of the map from R6 to R3 in each case. We define $v = [r_l, g_l, b_l, r_r, g_r, b_r]^T$ which are the RGB coordinates of the left and right eye color channels. The linear algorithms compute $[r, g, b]^T = Bv$. The linear methods differ only in the matrix B used to compute the map.

If a method produces colors that are not representable on the display (a coordinate lies outside the interval [0, 1]), clipping (projection) is used. Clipping maps nonrepresentable colors to the surface of the 3-cube. A projection map is linear.

Region merging occurs when adjacent regions of different colors are mapped to the same anaglyph color. This can affect depth and detail perceived in stereo images[13]. We note that clipping can cause region merging.

The spectral distributions of the phosphors on CRTs are shown in Figure 1.3(a). They have been uniformly scaled so the maximum value of red is 1. We also include the spectral distributions of the primaries for LCD monitors in Figure 1.3(b).

The conversion from RGB space to CIE space requires a linear transformation represented by the matrix C. The matrices C_{CRT} and C_{LCD} for the CRT and LCD spectral distributions in Figures 1.3(a) and 1.3(b) are

$$C_{CRT} = \begin{pmatrix} X_R & X_G & X_B \\ Y_R & Y_G & Y_B \\ Z_R & Z_G & Z_B \end{pmatrix} = \begin{pmatrix} 11.6638 & 8.3959 & 4.65843 \\ 7.10807 & 16.6845 & 2.45008 \\ .527874 & 3.79124 & 24.0604 \end{pmatrix}$$

and

$$C_{LCD} = \begin{pmatrix} X_R & X_G & X_B \\ Y_R & Y_G & Y_B \\ Z_R & Z_G & Z_B \end{pmatrix} = \begin{pmatrix} 0.4243 & 0.3105 & 0.1657 \\ 0.2492 & 0.6419 & 0.1089 \\ 0.0265 & 0.1225 & 0.8614 \end{pmatrix}$$

The discussions below are focused on LCD displays, so in the following discussion we let the conversion matrix $C = C_{LCD}$.

The gamut (on the CIE chromaticity diagram) for the spectral distributions of CRT monitors given in Figure1.3(a) is the RGB triangle in Figure1.5. The spectral distributions of CRT monitors have a similar gamut.

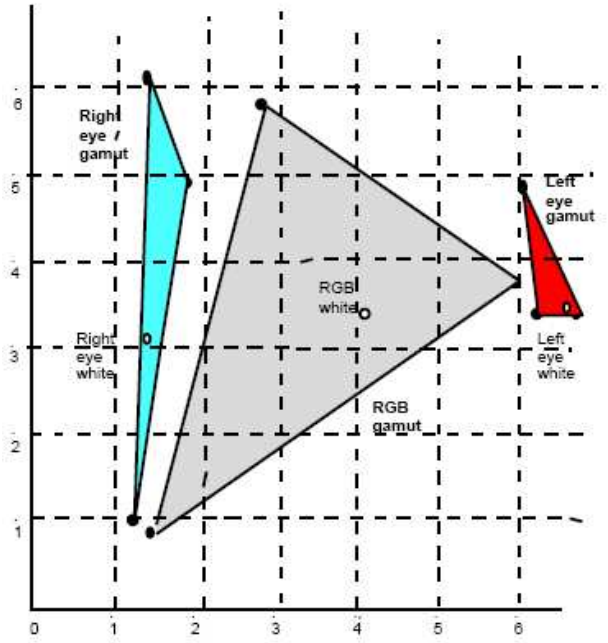

Figure 1.5: Gamuts in CIE space

1.3.3 Photoshop and Modified Photoshop Algorithms

In the original Photoshop algorithm [17] (PS) the red channel of the left eye view becomes the red channel of the anaglyph and vice versa for the blue and green channels of the right eye. This is equivalent to projecting the left eye RGB point to the red axis of the RGB cube (setting the G and B channels to zero) and the right eye RGB point to the GB plane (thus setting the red channel to zero). See Figure 8. The two resulting vectors are added to compute the color of the pixel in the anaglyph. This method is linear. The matrix B is

$$B = \begin{pmatrix} 1 & 0 & 0 & 0 & 0 & 0 \\ 0 & 0 & 0 & 0 & 1 & 0 \\ 0 & 0 & 0 & 0 & 0 & 1 \end{pmatrix}$$

The algorithm ignores the transmission function of the glasses, which means the computed anaglyph is the same for all filters. Another observation is that all colors with the same left eye red channel and the same blue/green channels in the right eye view will be mapped to the same color.

As a variant of the PS method, the modified photoshop algorithm (MPS) converts the left eye image to grayscale first and then projects as described above. If we use a linear grayscale conversion algorithm (such as the NTSC luminance standard where grayscale = .299r + .587g + .114b [3]) we premultiply v by a partitioned matrix of the form $\begin{pmatrix} G & 0 \\ 0 & I \end{pmatrix}$ where I is the 3x3 identity and G is the matrix $G = \begin{pmatrix} \alpha_1 & \alpha_1 & \alpha_1 \\ 0 & 1 & 0 \\ 0 & 0 & 1 \end{pmatrix}$ where the α_i' s are nonnegative, sum to 1, and are the coefficients that convert the red channel to grayscale. We then apply the matrix B above. This gives the new matrix

$$B = \begin{pmatrix} \alpha_1 & \alpha_2 & \alpha_3 & 0 & 0 & 0 \\ 0 & 0 & 0 & 0 & 1 & 0 \\ 0 & 0 & 0 & 0 & 0 & 1 \end{pmatrix}$$

No clipping is required.

1.3.4 Least Squares Algorithm

While the PS and MPS methods ignore the transmission properties of the filters, actually the colors visible through a filter depend on the transmission function $f(\lambda)$ of the filter. As discussed in section 1.2, the function f specifies the percentages of each visible wavelength λ transmitted by the filter. The product of the primary spectral distribution with the transmission function gives the spectral distribution of the primary as seen through the filter. The matrices Al for the left eye and Ar for the right eye convert the resulting filtered colors to CIE coordinates. For some common red/cyan glasses used below, these conversion matrices are:

$$Al = \begin{pmatrix} 0.1840 & 0.0179 & 0.0048 \\ 0.0876 & 0.0118 & 0.0018 \\ 0.0005 & 0.0012 & 0.0159 \end{pmatrix}, Ar = \begin{pmatrix} 0.0153 & 0.1092 & 0.1171 \\ 0.0176 & 0.3088 & 0.0777 \\ 0.0201 & 0.1016 & 0.6546 \end{pmatrix}$$

In[5] Eric Dubois showed how to use the transmission properties and spectral distributions for approximating colors in CIE color space to compute anaglyph colors. Dubois defined the length of a vector $\mathbf{x}$ = [X, Y, Z] in CIE space, using the Euclidean norm, $\|\mathbf{x}\|_2 = (X^2 + Y^2 + Z^2)^{\frac{1}{2}}$. The distance between two points x_1 and x_2 is therefore $\|x_1 - x_2\|_2$. In this case determining the closest vector in a subspace to a point not in the subspace is called least squares approximation (LS); the CIE color space is a linear space and approximation can be accomplished by a simple matrix multiplication for each pixel. LS approximation is equivalent to a projection in **R6** to the 3D subspace spanned by the 6 dimensional columns of the partitioned 6 x 3 matrix R defined below with right hand side partitioned vector d. The matrix C is the RGB-CIE conversion matrix defined above and v is the 6 component vector consisting of the left eye RGB color C_L and the right eye color C_R, $v = [C_L, C_R]^T$:

$$R = \begin{pmatrix} A_l \\ A_r \end{pmatrix}, d = \begin{pmatrix} C & 0 \\ 0 & C \end{pmatrix} v \tag{1.1}$$

The projection minimizes the Euclidean length of the vector $R[r, g, b]^T - d$.

This algorithm also uses scaling by a diagonal matrix N so that the white vector

$w_3 = [1,1,1]^T$ in **R3** is mapped to the white/white vector $w_6 = [1,1,1,1,1,1]^T$ in **R6**. The linear map can be written as $[r,g,b]^T = N(R^TR)^{-1}R^Td = Bv$. The diagonal matrix N can be computed from the equation $w_3^T = N(R^TR)^{-1}R^Tw_6^T$. The B matrices for LS approximation is

$$B = \begin{pmatrix} 0.4154 & 0.4710 & 0.1669 & -0.0109 & -0.0364 & -0.0060 \\ -0.0458 & -0.0484 & -0.0257 & 0.3756 & 0.7333 & 0.0111 \\ -0.0547 & -0.0615 & 0.0128 & -0.0651 & -0.1287 & 1.2971 \end{pmatrix}$$

We note that the approximation may result in RGB components that are out of range. That is, some may be negative and some may exceed 1. Dubois recommends clipping to the RGB unit cube to solve this problem. Although this process involves a trivial computation, applying it to every pixel in an image adds to the time complexity. In addition, the method produces images that can be a bit dark. It does not preserve color equality as the Photoshop method does. That is, if $C_L = C_R$, it is not necessarily the case that the optimal solution is $[r,g,b]^T = C_L$. In Figure 1.6(a) we have chosen equally spaced colors in the RGB cube for $C_L = C_R$. Figure1.6(b) shows the optimal solutions in the RGB cube. Note how the solutions have been mapped to a parallelepiped and many lie outside the unit RGB cube.

Greyscale, however, is preserved in the sense that if v is a (nonnegative) scalar multiple of white, $v = \alpha W$, then the optimal solution is also a scalar multiple of white. This follows from the properties of norms and the fact that matrix multiplication is linear: $B(\alpha w_6) = \alpha B w_6$ and $\|Ax - \alpha y\| = \alpha\|A(\frac{1}{\alpha}x) - y\|, \alpha > 0$.

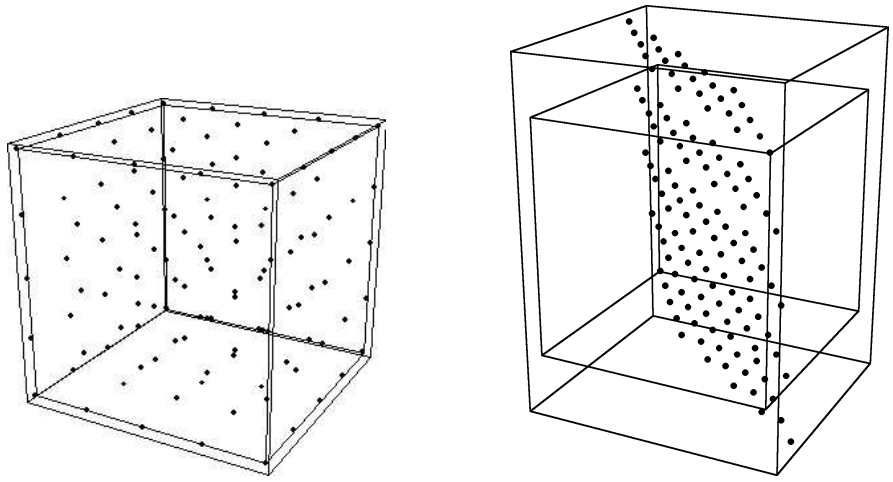

(a) Equally spaced colors in RGB (b) Images of points in part (a)

Figure 1.6: Images of equally spaced color points

Chapter 2

Uniform Anaglyph Calculation

2.1 Uniform Calculation Algorithm

2.1.1 A Revision of the LS Method

Another way to view the problem of anaglyph calculation is to consider it as trying to solve a system of equations. For each pixel of an anaglyph there are three unknowns to be calculated, namely the red, green, and blue values of the color at that pixel. The constraints to be satisfied are the red, green, and blue values that should be transmitted to the left and right eyes of the viewer through the filters. Recall from section 1.3.4 that if the red, green, and blue values at a pixel of an anaglyph are represented as a vector $[r, g, b]^T$, then the colors seen through the filters are described by the 6 dimensional vector $R[r, g, b]^T$; the colors that the left and right eyes of a viewer should see are described by the vector d where matrix R and vector d are defined in equation 1.1.

The goal of anaglyph calculation is to find r, g, b values such that:

$$R[r, g, b]^T = d \tag{2.1}$$

This is a system of 3 unknowns and 6 linear equations, which is an over-determined linear system. We discussed in section 1.3.4 that the LS method tries to find the closest vector in a subspace to a point that is possibly not in the subspace. In view of Equation 2.1

we can see that LS method actually tries to determine a vector in the range space of matrix R that is closest to the point d. That is equivalent to calculating the least squares solution of the system, and can be done by pre-multiplying the right-hand side vector d with the Moore-Penrose pseudoinverse of matrix R (scaled by the matrix N so that the white vector in **R6** is mapped to the white vector in **R3**).

2.1.2 Approximating in the Uniform Metric

Based on the LS method, we attempt to produce better color results by calculating approximate solutions to the system in Equation 2.1 using another metric. Thus we change the length measure or the norm to the *Chebychev*, *minimax*, *infinity* or *uniform* norm of a vector $\mathbf{x}$ and define $\|x\|_\infty = \max\{|X|, |Y|, |Z|\}$. Approximation is in CIE space as in the Dubois calculation but we minimize the length of the vector $R[r, g, b]^T - d$ using the uniform norm (UN) instead.

Using the uniform metric in this problem has an intuitive advantage compared with using the Euclidean metric. The 6 equations in the linear system in Equation 2.1 represent the relations between the red, green, and blue values the viewer's left and right eye should see and the values that his/her left and right eyes actually see when viewing an anaglyph through filters. While the LS method minimizes the square-sum of the 6 differences between the ideal values and the actual values, the UN method minimizes the maximal value among those 6 differences. Thus if we use the UN method, the total error will be more evenly distributed among the 6 equations.

As in the LS case, we want to ensure that the white vector $w_3 = [1, 1, 1]^T$ in **R3** is mapped to the white/white vector $w_6 = [1, 1, 1, 1, 1, 1]^T$ in **R6**. Instead of normalizing in the RGB space as the LS method does, we normalize in the CIE space. In other words, we compute the diagonal normalization matrix N such that $Rw_3 = Nw_6$, which gives $N =$ Diag[6.60522, 3.23678, 0.00263908, 4.02254, 8.12129, 12.624]. To minimize the maximum deviation, we use a 7th variable ϵ and we formulate the approximation problem as a *linear programming* problem (LP), which will be studied in more detail in section 2.2:

$$\begin{aligned} &\textit{minimize} \quad \epsilon \textit{ subject to the constraints } (s.t.): \\ &|(R[r, g, b]^T - Nd)_i| \leq \epsilon, 1 \leq i \leq 6 \\ &r, g, b \leq 1 \end{aligned} \tag{2.2}$$

The *simplex method* for solving LPs, which will be introduced in section 2.2.2, computes only nonnegative solutions. Since ϵ is bounded below automatically, the problem becomes a 7-variable LP with 15 constraints (the absolute value constraints are converted to two constraints each).

We can write the constraints as follows:

$$\begin{aligned} &minimize \quad \epsilon \ subject\ to\ the\ constraints\ (s.t.): \\ &-\epsilon \leq R[r,g,b]^T - Nd)_i \leq \epsilon, 1 \leq i \leq 6 \\ &r, g, b \leq 1 \end{aligned} \tag{2.3}$$

where all variables are nonnegative.

As in the LS case it does not preserve color equality. The bounds on r, g, and b prevent us from using the same argument as in the LS case, but numerical experiments suggest that it does preserve greyscale.

2.2 Background of Linear Programming

As stated above, Equation 2.2 is a *linear programming* problem (LP). According to [2], *linear programming* is the problem of minimizing a linear cost function subject to linear equality and inequality constraints. A general linear programming problem can always be transformed into an equivalent problem in the following form:

$$\begin{aligned} &minimize \quad c^T x \ \ s.t. \\ &Ax \leq b \\ &x \ \ unrestricted \end{aligned} \tag{2.4}$$

In the following sections (2.2.1, 2.2.2 and 2.2.3) we will introduce concepts and methods for solving LPs. For the convenience of discussion we assume that the matrix A always has linearly independent rows.

2.2.1 Geometry of Linear Programming

Polyhedra play an important role in the development of the *simplex method* so we will first introduce the formal definition of a polyhedron in [2]:

Definition 2.2.1 *A **polyhedron** is a set that can be described in the form* $\{\boldsymbol{x} \in \Re^n \mid \boldsymbol{A}\boldsymbol{x} \leq \boldsymbol{b}\}$*, where* $\boldsymbol{A}$ *is an* $m \times n$ *matrix and* $\boldsymbol{b}$ *is a vector in* $\Re^m$*.*

According to Definition 2.2.1 it can be seen that the *feasible region* of an LP in the form 2.4, i.e., the set of all points $\mathbf{x}$ that satisfy the constraint functions $Ax \leq b$, is a polyhedron. It is observed from simple LP examples that the optimal solutions are always obtained at the "corners" of the feasible regions, which are polyhedra. In order to establish this fact, first we need the mathematical definition of "corners" of polyhedra. Two important geometric concepts, *extreme points* and *vertices* [2], are defined below.

Definition 2.2.2 *Let* P *be a polyhedron. A vector* $\boldsymbol{x} \in P$ *is an **extreme point** of* P *if we cannot find two vectors* $\boldsymbol{y}, \boldsymbol{z} \in P$*, both different from* $\boldsymbol{x}$*, and a scalar* $\lambda \in [0, 1]$*, such that* $x = \lambda y + (1 - \lambda)z$*.*

An example is shown in Figure 2.1(a). For any two points y and z in the polyhedron, x is not on the line segment that joins them, in other words, x is an extreme point of the polyhedron.

Definition 2.2.3 *Let* P *be a polyhedron. A vector* $\boldsymbol{x} \in P$ *is a **vertex** of* P *if there exists some vector* $\boldsymbol{c}$ *such that* $c^T\ \boldsymbol{x} < c^T\ \boldsymbol{y}$ *for all* y *satisfying* $\boldsymbol{y} \in P$ *and* $\boldsymbol{y} \neq \boldsymbol{x}$*.*

In view of the above definition, the point x in Figure 2.1(b) is a vertex of the polyhedron, because for the vector c shown in this figure, $c^T x < c^T y$ for any point $y \neq x$ in the polyhedron.

To establish the relation between optimal solutions and "corners" of polyhedra, we also need to introduce the concept of *basic feasible solutions* (BFS) [2] of an LP as follows:

Definition 2.2.4 *Consider a polyhedron* P *defined by linear equality and inequality constraints, and let* $\boldsymbol{x^*}$ *be an element of* $\Re^n$*. We say an equality constraint is* active *if it is satisfied (holds); we say an inequality constraint is active if it is satisfied and the corresponding equality holds.*

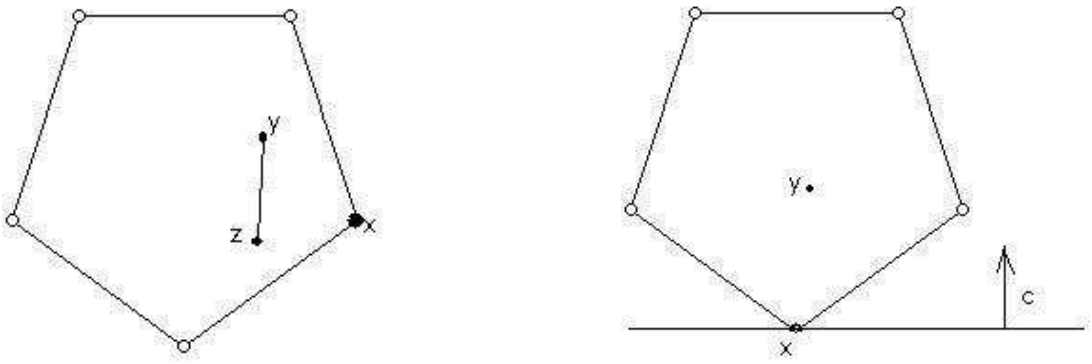

(a) Extreme point (b) Vertex

Figure 2.1: A vertex and a extreme point of a polyhedron

(a) The vector x is a* ***basic solution*** *if:*

(i) All equality constraints are active;

(ii) Out of the constraints that are active at ***x****, there are n of them that are linearly independent.*

(b) If ***x**** *is a basic solution that satisfies all of the constraints, we say that it is a* ***basic feasible solution****.*

It is shown in [2] that: a vector **x*** is a vertex of a polyhedron P $\iff$ (if and only if) **x*** is an extreme point of P $\iff$ x* is a basic feasible solution of P. It is further proven that if the linear programming problem of minimizing $\mathbf{c}^T\mathbf{x}$ over a polyhedron P has at least one optimal solution, and P has at least one extreme point, then there exists an optimal solution which is an extreme point. This conclusion, together with the observation that a polyhedron in standard form 2.4 always has at least one extreme point, verifies the approach of finding the optimal solution of an LP by checking the cost function value for all the extreme points of the feasible region, which are in finite number.

2.2.2 The Simplex Method

A common approach for solving an LP is the simplex method. The simplex method is based on the conclusion we made in section 2.2.1 and searches for an optimal solution by moving from one basic feasible solution to another, along the edges of the feasible set, always in a cost reducing direction [2]. Figure 2.2[4] gives a simple illustration of how the simplex method works, where the green area is the feasible region.

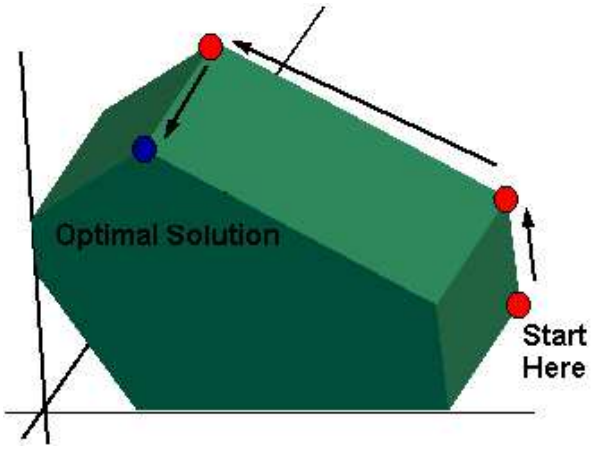

Figure 2.2: The simplex algorithm

In order to develop and implement the simplex method, we need to introduce the procedure of constructing basic feasible solutions and the mechanism of moving from one basic feasible solution to another with reduced cost. First we need to introduce the following standard form for an LP:

$$\begin{aligned} minimize \quad & c^T x \quad s.t. \\ & Ax = b \\ & x \geq 0 \end{aligned} \tag{2.5}$$

As argued in [2], any LP in form 2.4 can be further converted to the above standard form. Furthermore, according to the following theorem from [2], we can construct all basic feasible solutions of an LP in standard form 2.5 with simple algebraic operations:

Theorem 2.2.1 *Consider the constraints* $\boldsymbol{Ax} = \boldsymbol{b}$ *and* $\boldsymbol{x} \geq 0$ *and assume that the* $m \times n$

matrix $\boldsymbol{A}$ *has linearly independent rows. A vector* $x \in \Re^n$ *is a basic solution if and only if we have* $\boldsymbol{Ax} = \boldsymbol{b}$*, and there exist indices* $B(1), \ldots, B(m)$ *such that:*

(a) The columns $\boldsymbol{A}_{B(1)}, \ldots, \boldsymbol{A}_{B(m)}$ *are linearly independent;*

(b) If $i \neq B(1), \ldots, B(m)$*, then* $x_i = 0$*.*

In view of the above theorem, all basic solutions to a standard form LP can be constructed by first choosing m linearly independent columns $\mathbf{A}_{B(1)}, \ldots, \mathbf{A}_{B(m)}$, then letting $x_i = 0$ for all $i \neq B(1), \ldots, B(m)$ and finally solving the system of m equations $\mathbf{Ax} = \mathbf{b}$ for the unknowns $\mathbf{x}_{B(1)}, \ldots, \mathbf{x}_{B(m)}$. If the basic solution constructed has all nonnegative components, then it is a basic feasible solution. The set of columns $B = \{\mathbf{A}_{B(1)}, \ldots, \mathbf{A}_{B(m)}\}$ forms a basis for the m dimensional linear space and is called the as the basis of the corresponding basic solution.

The simplex method moves from one basic feasible solution to another by taking one column out of the current basis and inserting a new column into it. If two bases are the different only for one column, then they are said to be *adjacent* bases and the corresponding basic feasible solutions are also said to be adjacent. Adjacent basic feasible solutions correspond to adjacent vertices of the feasible region of the LP. Thus the simplex method moves from one vertex to an adjacent one with reduced cost. If all adjacent vertices are with higher costs than the current one, then the optimum is achieved. An anti-circling scheme is used so that the algorithm will never consider a previously visited vertex. This scheme, combined with the fact that there are always finite number of vertices in the polygon, guarantees that the simplex algorithm finds the optimum in a finite number of steps.

2.2.3 Conclusion

In many cases the simplex algorithm is not the best approach to solve linear programming problems. While being conceptually elegant, it takes $O(2^n)$ running time in the worst case, where all vertices of the feasible region are visited before the optimal solution is found out. The exponential complexity makes it inefficient for large scale problems. Around the early 1980's algorithms with polynomial running time were developed. One

important example is the interior point method introduced in [10]. Instead of moving from one vertex to another along edges like the simplex algorithm, the interior method goes through the interior of the polyhedral feasible region to find the optimal solution.

While the interior algorithm has a better asymptotic complexity, the simplex algorithm has less cost for a single step. In our problem the small size of the LP justifies using the simplex algorithm. However, as we will discuss in chapter 5, applying the interior point method has a potential of bringing about a further acceleration of the calculation, and it is a direction of our future research.

Generally speaking, solving an LP is considerably more computationally complex than applying a single matrix multiplication. Hence the problem produces interesting computational issues and in section 3 we seek parallel computation methods to accelerate the calculation to take advantage of coherence in digital images: the optimal solution at a given pixel is normally close to the optimal solutions of the surrounding pixels and the optimal solution for a pixel in a given frame of video is usually close to the optimal solution in the succeeding frame. Our goal is to produce anaglyphs of video signals at NTSC rates so we can apply the technique to problems like distance learning and virtual laboratories.

2.3 Color and Performance of the Uniform Method

2.3.1 Color Test

We compare the color, brightness and ghosting qualities of four algorithms: UN, LS, PS, and MPS. We created Gouraud shaded ellipsoids using 3D Studio. The hue and saturation over a given ellipsoid are the same for all pixels, but brightness varies from approximately 0 to 100 percent.

All ellipsoids are about the same size and the same distance from the viewer. We chose 64 RGB values that were equally spaced over the RGB cube, grouping them eight at a time. The colors are the coordinates of vertices of subcubes with edge lengths approximately $\frac{255}{3} \cong 85$. We consider all permutations of the intensities of 0, 85, 171 and 255 taken 3 at a time. The background is set to a neutral gray intensity of 166. There is no gamma correction. The cubes are numbered as shown in Table 2.1:

As an example, the images for cube 6 are shown in Figure 2.3. Images for other

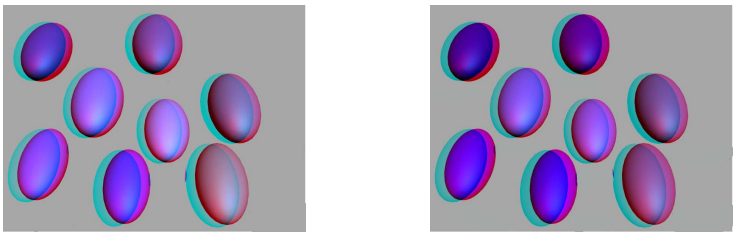

(a) LS

(b) MPS

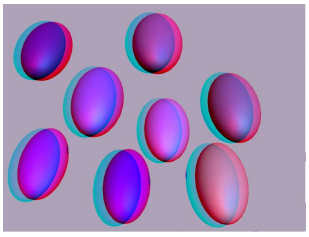

(c) UN

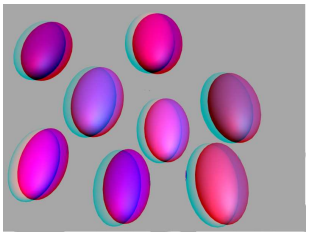

(d) PS

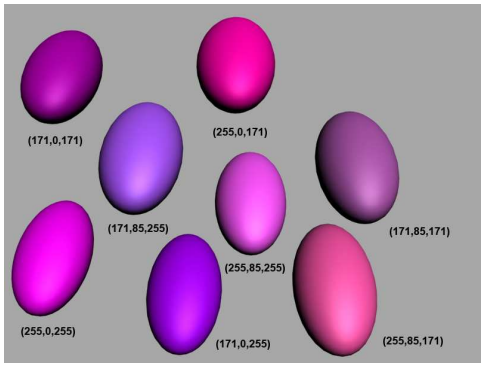

(e) Left eye view with true color

Figure 2.3: Cube 6 - Stereo image rendered with different methods

Table 2.1: Cube numbering scheme

Cube number	R	G	B
Cube 1	0, 85	0, 85	0, 85
Cube 2	171, 255	0, 85	0, 85
Cube 3	171, 255	171, 255	0, 85
Cube 4	0, 85	171, 255	0, 85
Cube 5	0, 85	0, 85	171, 255
Cube 6	171, 255	0, 85	171, 255
Cube 7	0, 85	171, 255	171, 255
Cube 8	171, 255	171, 255	171, 255

cubes are given in Appendix A. We note for cube 6 the significant color differences produced by the methods when viewed without using anaglyph filters

2.3.2 Color Results

We did not attempt to perform a study in which the results were statistically significant since the effect of retinal rivalry cannot be predicted nor controlled. However, the comparisons for three non-colorblind observers were consistent, so we report them here. We compare each ellipsoid with the original left or right eye view *with glasses* (we note that comparing colors without the glasses is pointless and can result in misleading conclusions). We used three different pairs of red/cyan glasses: Reel3-D No. 7003, IMAX Fujitsu and the glasses provided by ABC to view the television show *Medium*. The results were independent of the glasses.

Our comparisons describe hue faithfulness except where noted. We also comment on brightness, ghosting[18] , and retinal rivalry[11] when the differences were significant. Since PS preserves color when the left and right eye values at a pixel are the same, we expect PS to be superior in hue and brightness approximation for most of the examples in our test. We comment below only when PS is not the best. Unfortunately, PS also inherits any problems with extreme retinal rivalry that exists when viewing the original left or right eye views through the filters. This phenomenon is apparent in Cubes 2 and 5 described below. Hence, our comparisons are primarily between UN, LS and MPS. Recall that the red channel of MPS is computed by converting the left eye view to grayscale and inserting it in the red channel of the anaglyph. In regions of low green and blue intensities, the weighted average of R, G and B used to compute the intensity of the red channel may decrease the

value of R in the anaglyph making the image darker. This phenomenon is evident in the results for Cube 2.

For cube 1 (Figure A.1), the point (0,0,0) or black, is the same for all methods, as was (0, 0, 85). UN is the best at points (85,0,0) and (85,0,85). PS is slightly worse, with MPS and LS equally bad. For (85,85,0), LS is only slightly better than MPS, and UN and PS are equally poor. LS is again the best for (0,85,0), then UN, then PS, and finally MPS. At (0,85,85) UN and LS are equally bad, and MPS is the worst. All are similar for the gray level (85,85,85) although UN is slightly darker.

For cube 2 (Figure A.2), shades of red, UN is best for all points. However, UN, while being a similar hue, is too bright, and there is conspicuous ghosting. LS and MPS are always too dark, but at points (171,0,0), (171, 85,85) and (255,0,0), LS is the worst, while MPS is worst at (255,0,85), (255,85,85), (171,0,85), and (255,85,0). MPS and LS are similar at (171,85,0). Retinal rivalry is a problem for PS.

Color cube 3 (Figure A.3) contains pale oranges and greens. The results are varied. At (171,171,0) UN is a similar hue, but too light. MPS is next in accuracy and LS worst. At (255,171,0), UN is again too bright, then LS, and MPS. UN, PS and MPS are equal, and LS is worst at (171,171,85) and (171,255,85). LS is best at (171,255,0), then MPS, and UN last. LS and MPS are almost the same at (255,255,0), and UN is the worst. At (255,171,85), UN is the best, followed by LS, then MPS. UN is consistently too light, but the hues are closer to the originals than the hues of MPS or LS.

Cube 4 (Figure A.4) is shades of green. UN is the best at (0,171,0). PS is second, MPS is too light, and LS is too dark. For the points (0,255,0), (85,171,0),(85,255,0), (0,171,85), (0,255,85), (85,171,85), and (85, 255,85), there is a large amount of ghosting and retinal rivalry in PS. UN is consistently second best for these points, with a slightly different hue, but with the least ghosting and retinal rivalry. MPS is third with a different hue and too light. LS is worst with a much darker intensity and a different hue.

Cube 5 (Figure A.5) is the blue region. All ellipsoids have severe ghosting and retinal rivalry. At (0,0,171), UN is best, followed by PS and MPS equally. LS is too light and the wrong hue. UN is again the most accurate at (85,0,171), PS is too light, LS is the wrong hue, and MPS is too dark and the wrong hue. UN is the best approximation at (0,85,171) and (0,85,255). PS is slightly light, and MPS and LS are about the same-too light and the wrong hue. At (85,85,255), UN is the best, then MPS, LS, and PS. Extreme retinal rivalry makes color determination difficult for PS at (85,0,255). For this case, UN is

second, then LS, and then MPS. PS is again the closest at (85,85,171), followed by MPS. UN and LS are equally too light and the wrong hue. The worst ghosting takes place at (0,0,255), with MPS best and the others almost impossible to see because of the retinal rivalry.

Cube 6 (Figure 2.3) contains the purple hues. UN is best for most cases. UN is best for (171,85,171) and (171,85,255), followed by PS which has more ghosting. LS and MPS were too dark, but MPS was the darkest. For the remaining points the order in decreasing hue approximation is UN, LS and MPS. For these remaining points there is significant retinal rivalry in PS. There is less retinal rivalry and ghosting is least for UN.

Cube 7 (Figure A.7) is the cyan region. There is considerable ghosting and retinal rivalry in PS. Second is MPS, with the right hue, but too light. LS is always the wrong hue, but the best brightness match. UN is consistently too dark and the wrong hue.

Cube 8 (Figure A.8) is the white corner of the RGB cube, the least saturated colors. All the methods produce approximately the same image for (171,171,171) and (255,255,255). All produce images of equal brightness at (171,171,255), but UN has a distinct rim in the ghosting area, an interesting phenomenon. At (171,255,171) LS is the wrong hue, MPS is worse, and UN is the worst but has the least amount of ghosting. UN is best at (255,171,171). LS is the wrong hue, and MPS is too dark and the wrong hue. At (255,255,171), MPS is best. LS is too bright, and UN is far too bright. There is considerable retinal rivalry in the PS approximation at (255,171,255), but it is the best hue approximation. UN and LS are about equal, and MPS is too dark. At (171,255,255) none of the three methods produces the correct hue. MPS is far too light, and UN is too dark.

No method is best for approximating all colors. The choice of a method depends on the colors involved, the importance of approximating brightness and the amount of ghosting produced. UN and PS were the most consistently accurate. PS is almost always better than MPS and requires the least calculation of all methods considered. LS usually produces a poor approximation for any hue. As mentioned above, retinal rivalry is severe in the cube 2 (reds) and 5 (blues) regions. We recommend avoiding these colors when possible. In most cases UN produces the least amount of ghosting and retinal rivalry without sacrificing brightness, a good reason to consider it in spite of the computational complexity discussed below. All the methods are good for unsaturated colors and for grayscale.

2.4 Computing Performances

As expected in section 2.2.3, the computation of UN method takes much more time than that of PS, MPS and LS methods. When we implement the calculation with Mathematica, it takes more than 3 hours to process a 1085×675 image on a Dell 700m laptop computer with a 1.6 GHz CPU and 512 M memory. The implementation in C++ language is much faster, but it still takes more than 2 minutes to process the same image. After testing the UN method on a set of images with different sizes, from 60030 to 856544 pixels, we find that the processing time is 1.5×10^{-4} to 2.5×10^{-4} seconds per pixel, the average being 1.9×10^{-4} seconds.

In contrast, the computations of the PS, MPS and LS methods are much faster. The same set of images are tested with the three methods. In all three cases the running time is nearly linear in the number of pixels. The processing time per pixel is approximately 3.6×10^{-7} seconds for the PS method, 5.3×10^{-7} seconds for the MPS method, and 1.27×10^{-6} seconds for the LS method. It can be seen that although all the 3 methods calculate a matrix-vector multiplication at each pixel, they have different processing speeds. This fact can be understood if we look at their different B matrices given in sections 1.3.3 and 1.3.4. Among the three matrices, the B matrix of the PS method is the sparsest, that is, it has the smallest number of non-zero entries; the B matrix of the MPS method is sparser than that of the LS method. The more zero entries there are in a matrix, the less time it is required to multiply it with a vector. Thus for these three methods, the processing speed is determined by the sparseness of the B matrix. Nevertheless, all these three methods are at least 100 times faster than the UN method.

Chapter 3

Accelerating the Calculation

In the discussion below, the conclusions are based on the behavior of our methods for several continuous tone photographs. Our computing environment for the uniprocessor case is a Dell 700m computer with 1.6 GHz CPU. Our parallel processing environment is an 8-node Cluster, where each node has dual 2.8-3.06 GHz processors. More specific information about the experimental environments and results can be found in section 4.

As stated in chapter 2, UN calculation is considerably more expensive computationally than the methods PS, MPS and LS, where only matrix multiplications are required. A stereo pair of 1085 by 675 images we test requires the unaccelerated UN method 127 seconds to render the anaglyph while the PS method requires less than 0.01 second. Our efforts to accelerate the UN calculation is described in the following sections.

3.1 Exploiting Color Coherence

3.1.1 Color Coherence in Real World Images

Coherence, or *locality of reference*, is an important concept in Computer Science. One example is the *spatial locality* in memory accessing, which refers to the higher likelihood of accessing a memory location if a location near it was just accessed. The *Cache* technique takes advantage of the spatial locality by pre-fetching data stored near the location currently

Figure 3.1: An example of color coherence

visited, so that future accesses are likely to find the desired data in the Cache.

As mentioned in [6], in computer graphics and image compression there are also many forms of coherence that are used to make rendering more efficient. In our case the color of a pixel is often *similar* to that of its neighbors, where being similar is defined as being close relative to a distance measure or metric in the color space being considered. Furthermore, there often exist sets of pixels with similar colors, and located as *connected regions* (defined below) in the image. An example is shown in Figure 3.1.

In our discussion an image is viewed as a 2D array of pixels. For a pixel q which lies in the i_{th} row and the j_{th} column, another pixel p is q's *neighbor* if p's row index is $i-1$, i, or $i+1$, and p's column index is $j-1$, j, or $j+1$. As shown in Figure 3.2, pixel q has 8 neighbors, namely $p_1, p_2, \ldots, p_8$. A set S of pixels forms a connected region if for any two pixels $p_0, p_n \in S$, there exist pixels $p_1, p_2, \ldots, p_{n-1} \in S$ such that p_i is a neighbor of p_{i+1} for $i = 0, 1, \ldots, n-1$.

The reason we want to introduce the concept of connected regions is that in most cases an image from real world applications is consist of many *semantic objects*. In image analysis a semantic object, or a *meaningful entity*, refers to an object whose parts have common interpretation such as a human face, the sky, a piece of clothing, and so forth.

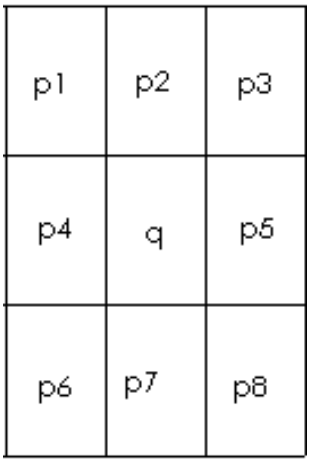

Figure 3.2: A pixel's neighbors

Semantic objects in an image do not generally have regular shapes, but in most cases each object occupies a connected region in the image. One example is the terraced field in Figure 3.1, where each terrace, although in very irregular shape, is a connected region with similar colors.

With the definition of connected regions we are able to recognize semantic objects and divide pixels with similar colors into groups. In section 3.1.3 an approach is developed to take each connected region with similar colors as a unit, solve an LP for each unit just once, and process all the pixels in the unit with matrix-vector multiplications.

3.1.2 Color Coherence and Linear Programming

Intuitively two pixels have close colors implies that the optimal solutions of the associated LPs should be "close" in the sense that solutions will often be the same or "adjacent" on the simplex defining the set of feasible solutions. We seek to find ways to exploit this in the simplex algorithm: after solving the LP for one pixel we try to use the solution to help process its neighbors faster, instead of executing the simplex algorithm for every pixel.

First an interesting fact should be noticed by observing equations 2.2: the linear programming problems for all pixels are similar in that they have the same objective function and constraint matrix, the only difference being the right hand values $\pm(Nd)_i$ of the

constraints when put in the standard form (2.5).

Moreover, according to Theorem 3.1.1 from [2], if the difference between each component of the right hand sides of two such problems is within a certain interval (specified below), and we have already computed the solution to one of the problems, then the other can be solved with a simple matrix-vector multiplication.

Theorem 3.1.1 *Let B be the basis of the current optimal solution, and $g = (\beta_{1i}, \beta_{2i}, \ldots, \beta_{mi})$ be the i_{th} column of B^{-1}. Suppose that the i_{th} component b_i of the right hand side vector b is changed to $b_i + \delta$, and δ satisfies:*

$$\max_{\{j|\beta_{ji}>0\}}(-\frac{x_{B(j)}}{\beta_{ji}}) \leq \delta \leq \min_{\{j|\beta_{ji}<0\}}(-\frac{x_{B(j)}}{\beta_{ji}})$$

For δ in this range, the new optimal solution has the same optimal basis as the old one, and the value is given by $c_B^T B^{-1}(b + \delta e_i)$, where c is the cost vector introduced in Equations 2.4 and 2.5, and $c_B = (c_{B(A)}, c_{B(2)}, \ldots, c_{B(m)})$ with $B(1), B(2), \ldots, B(m)$ being the indices of the current basis.

In our specific problem the difference between the right hand sides of two linear programming problems depends on the difference between the colors of the two corresponding pixels. Thus if two pixels have similar colors, their associated LPs have the same optimal basis.

We use a numerical example to illustrate this. For a pixel with left eye color (r_l, g_l, b_l) and right eye color (r_r, g_r, b_r), the linear programming problem is given by:

$$\begin{aligned} &minimize \;\; \epsilon \quad s.t \\ &-\epsilon \leq R[r,g,b] - Nd)_i \leq \epsilon, 1 \leq i \leq 6 \\ &r, g, b \leq 1, \end{aligned}$$

where $d = \begin{pmatrix} C & 0 \\ 0 & C \end{pmatrix} \cdot [r_l, g_l, b_l, r_r, g_r, b_r]^T$. In order to apply the simplex algorithm, we need to transform the LP into the standard form introduced in Equation 2.5. The above

LP has 15 inequality constraints and 4 variables $\epsilon, r, g,$ and b. We denote $\epsilon, r, g,$ and b by $x_1, x_2, x_3,$ and x_4, respectively. For each inequality equation $\alpha_1 x_1 + \alpha_2 x_2 + \alpha_3 x_3 + \alpha_4 x_4 \leq b$, if we introduce a slack variable x_s which is restricted to be nonnegative, we can get the equivalent form $\alpha_1 x_1 + \alpha_2 x_2 + \alpha_3 x_3 + \alpha_4 x_4 + x_s = b, x_s \geq 0$. Thus by introducing one slack variable for each inequality, the LP can be transformed into the the standard form given below:

$$\begin{aligned} &minimize \;\; x_1 \quad s.t. \\ &E[x_1, x_2, x_3, x_4, x_5, \ldots, x_{19}]^T = \quad F[r_l, g_l, b_l, r_r, g_r, b_r, 1, 0, 0]^T \\ &x_1, x_2, x_3, x_4, x_5, \ldots, x_{19} \geq 0 \end{aligned} \tag{3.1}$$

The matrices E and F are given below:

$$E = \begin{pmatrix} -1 & -5.423 & -0.807 & -0.047 & 1 & 0 & 0 & 0 & 0 & 0 & 0 & 0 & 0 & 0 & 0 & 0 & 0 & 0 \\ -1 & -2.710 & -0.502 & -0.025 & 0 & 1 & 0 & 0 & 0 & 0 & 0 & 0 & 0 & 0 & 0 & 0 & 0 & 0 \\ -1 & -0.00006 & -0.0004 & -0.002 & 0 & 0 & 1 & 0 & 0 & 0 & 0 & 0 & 0 & 0 & 0 & 0 & 0 & 0 \\ -1 & -0.180 & -1.640 & -2.003 & 0 & 0 & 0 & 1 & 0 & 0 & 0 & 0 & 0 & 0 & 0 & 0 & 0 & 0 \\ -1 & -0.448 & -6.315 & -1.358 & 0 & 0 & 0 & 0 & 1 & 0 & 0 & 0 & 0 & 0 & 0 & 0 & 0 & 0 \\ -1 & -0.289 & -2.393 & -11.062 & 0 & 0 & 0 & 0 & 0 & 1 & 0 & 0 & 0 & 0 & 0 & 0 & 0 & 0 \\ -1 & 5.423 & 0.807 & 0.047 & 0 & 0 & 0 & 0 & 0 & 0 & 1 & 0 & 0 & 0 & 0 & 0 & 0 & 0 \\ -1 & 2.710 & 0.502 & 0.025 & 0 & 0 & 0 & 0 & 0 & 0 & 0 & 1 & 0 & 0 & 0 & 0 & 0 & 0 \\ -1 & 0.00006 & 0.0004 & 0.002 & 0 & 0 & 0 & 0 & 0 & 0 & 0 & 0 & 1 & 0 & 0 & 0 & 0 & 0 \\ -1 & 0.180 & 1.640 & 2.003 & 0 & 0 & 0 & 0 & 0 & 0 & 0 & 0 & 0 & 1 & 0 & 0 & 0 & 0 \\ -1 & 0.448 & 6.316 & 1.358 & 0 & 0 & 0 & 0 & 0 & 0 & 0 & 0 & 0 & 0 & 1 & 0 & 0 & 0 \\ -1 & 0.289 & 2.393 & 11.062 & 0 & 0 & 0 & 0 & 0 & 0 & 0 & 0 & 0 & 0 & 0 & 1 & 0 & 0 \\ 0 & 1 & 0 & 0 & 0 & 0 & 0 & 0 & 0 & 0 & 0 & 0 & 0 & 0 & 0 & 0 & 1 & 0 \\ 0 & 0 & 1 & 0 & 0 & 0 & 0 & 0 & 0 & 0 & 0 & 0 & 0 & 0 & 0 & 0 & 0 & 1 \\ 0 & 0 & 0 & 1 & 0 & 0 & 0 & 0 & 0 & 0 & 0 & 0 & 0 & 0 & 0 & 0 & 0 & 1 \end{pmatrix}$$

$$F = \begin{pmatrix} -3.0655 & -2.0179 & -1.1942 & 0 & 0 & 0 & 0 & 0 & 0 \\ -0.8406 & -2.1337 & -0.2625 & 0 & 0 & 0 & 0 & 0 & 0 \\ -0.0001 & -0.0004 & -0.0024 & 0 & 0 & 0 & 0 & 0 & 0 \\ 0 & 0 & 0 & -1.8669 & -1.2289 & -0.7273 & 0 & 0 & 0 \\ 0 & 0 & 0 & -2.1091 & -5.3536 & -0.6586 & 0 & 0 & 0 \\ 0 & 0 & 0 & -0.4507 & -1.7939 & -11.4992 & 0 & 0 & 0 \\ 3.0655 & 2.0179 & 1.1942 & 0 & 0 & 0 & 0 & 0 & 0 \\ 0.8406 & 2.1337 & 0.2625 & 0 & 0 & 0 & 0 & 0 & 0 \\ 0.0001 & 0.0004 & 0.0024 & 0 & 0 & 0 & 0 & 0 & 0 \\ 0 & 0 & 0 & 1.8669 & 1.2289 & 0.7273 & 0 & 0 & 0 \\ 0 & 0 & 0 & 2.1091 & 5.3536 & 0.6586 & 0 & 0 & 0 \\ 0 & 0 & 0 & 0.4507 & 1.7939 & 11.4992 & 0 & 0 & 0 \\ 0 & 0 & 0 & 0 & 0 & 0 & 1 & 0 & 0 \\ 0 & 0 & 0 & 0 & 0 & 0 & 1 & 0 & 0 \\ 0 & 0 & 0 & 0 & 0 & 0 & 1 & 0 & 0 \end{pmatrix}$$

For a pixel p_{old} with left eye color (247, 231, 206) and right eye color (55, 20, 27), the indices of the optimal basis B are

$$[B(1), B(2), \ldots, B(15)] = [1, 6, 7, 8, 9, 2, 11, 12, 13, 14, 3, 16, 4, 18, 19]$$

. The basis and its inverse are given below:

$$B = \begin{pmatrix}
-1 & 0 & 0 & 0 & 0 & -5.423 & 0 & 0 & 0 & 0 & -0.807 & 0 & -0.047 & 0 & 0 \\
-1 & 1 & 0 & 0 & 0 & -2.710 & 0 & 0 & 0 & 0 & -0.502 & 0 & -0.025 & 0 & 0 \\
-1 & 0 & 1 & 0 & 0 & -0.00006 & 0 & 0 & 0 & 0 & -0.0004 & 0 & -0.002 & 0 & 0 \\
-1 & 0 & 0 & 1 & 0 & -0.180 & 0 & 0 & 0 & 0 & -1.640 & 0 & -2.003 & 0 & 0 \\
-1 & 0 & 0 & 0 & 1 & -0.448 & 0 & 0 & 0 & 0 & -6.315 & 0 & -1.358 & 0 & 0 \\
-1 & 0 & 0 & 0 & 0 & -0.289 & 0 & 0 & 0 & 0 & -2.393 & 0 & -11.062 & 0 & 0 \\
-1 & 0 & 0 & 0 & 0 & 5.423 & 1 & 0 & 0 & 0 & 0.807 & 0 & 0.047 & 0 & 0 \\
-1 & 0 & 0 & 0 & 0 & 2.710 & 0 & 1 & 0 & 0 & 0.502 & 0 & 0.025 & 0 & 0 \\
-1 & 0 & 0 & 0 & 0 & 0.00006 & 0 & 0 & 1 & 0 & 0.0004 & 0 & 0.002 & 0 & 0 \\
-1 & 0 & 0 & 0 & 0 & 0.180 & 0 & 0 & 0 & 1 & 1.640 & 0 & 2.003 & 0 & 0 \\
-1 & 0 & 0 & 0 & 0 & 0.448 & 0 & 0 & 0 & 0 & 6.316 & 0 & 1.358 & 0 & 0 \\
-1 & 0 & 0 & 0 & 0 & 0.289 & 0 & 0 & 0 & 0 & 2.393 & 1 & 11.062 & 0 & 0 \\
0 & 0 & 0 & 0 & 0 & 1 & 0 & 0 & 0 & 0 & 0 & 0 & 0 & 0 & 0 \\
0 & 0 & 0 & 0 & 0 & 0 & 0 & 0 & 0 & 0 & 1 & 0 & 0 & 1 & 0 \\
0 & 0 & 0 & 0 & 0 & 0 & 0 & 0 & 0 & 0 & 0 & 0 & 1 & 0 & 1
\end{pmatrix}$$

$$B^{-1} = \begin{pmatrix}
-0.874 & 0 & 0 & 0 & 0 & -0.01 & 0 & 0 & 0 & 0 & -0.116 & 0 & -4.69 & 0 & 0 \\
-0.953 & 1 & 0 & 0 & 0 & -0.004 & 0 & 0 & 0 & 0 & -0.0436 & 0 & -2.439 & 0 & 0 \\
-0.874 & 0 & 1 & 0 & 0 & -0.011 & 0 & 0 & 0 & 0 & -0.116 & 0 & -4.6890 & 0 & \\
-0.912 & 0 & 0 & 1 & 0 & -0.167 & 0 & 0 & 0 & 0 & 0.08 & 0 & -4.851 & 0 & 0 \\
-1.748 & 0 & 0 & 0 & 1 & -0.021 & 0 & 0 & 0 & 0 & 0.769 & 0 & -9.38 & 0 & 0 \\
0 & 0 & 0 & 0 & 0 & 0 & 0 & 0 & 0 & 0 & 0 & 0 & 1 & 0 & 0 \\
-0.748 & 0 & 0 & 0 & 0 & -0.021 & 1 & 0 & 0 & 0 & -0.231 & 0 & -9.381 & 0 & 0 \\
-0.795 & 0 & 0 & 0 & 0 & -0.017 & 0 & 1 & 0 & 0 & -0.188 & 0 & -6.942 & 0 & 0 \\
-0.874 & 0 & 0 & 0 & 0 & -0.010 & 0 & 0 & 1 & 0 & -0.116 & 0 & -4.691 & 0 & 0 \\
-0.836 & 0 & 0 & 0 & 0 & 0.146 & 0 & 0 & 0 & 1 & -0.311 & 0 & -4.529 & 0 & 0 \\
-0.163 & 0 & 0 & 0 & 0 & 0.018 & 0 & 0 & 0 & 0 & 0.144 & 0 & -0.943 & 0 & 0 \\
-1.748 & 0 & 0 & 0 & 0 & 0.979 & 0 & 0 & 0 & 0 & -0.231 & 1 & -9.38 & 0 & 0 \\
0.114 & 0 & 0 & 0 & 0 & -0.093 & 0 & 0 & 0 & 0 & -0.021 & 0 & 0.602 & 0 & 0 \\
0.163 & 0 & 0 & 0 & 0 & -0.018 & 00 & 0 & 0 & -0.144 & 0 & -0.057 & 1 & 0 & \\
-0.114 & 0 & 0 & 0 & 0 & 0.093 & 0 & 0 & 0 & 0 & 0.021 & 0 & -0.602 & 0 & 1
\end{pmatrix}$$

Consider a pixel p_{new} with left eye color (247, 231, 206) and right eye color (55, 20, 21). Compared with p_{old}, the only difference is that b_r is changed from 27 to 21. This difference causes changes to the $4_{th}, 5_{th}, 6_{th}, 10_{th}, 11_{th}$, and 12_{th} components of the right hand side vector. The 4_{th} component is changed from -146.9 to -142.5, i.e., $\delta = 4.4$. The 4_{th} column of B^{-1} is $[0,0,0,1,0,0,0,0,0,0,0,0,0,0,0]^T$, i.e., $\beta_{44} = 1$ and $\beta_{j4} = 0$ for $j \neq 4$. Because all variables in the solution are nonnegative, we can see that $\delta \geq 0 \geq -\frac{x_{B(4)}}{\beta_{44}}$. Then δ satisfies the condition specified in Theorem 3.1.1. Therefore we know that p_{new} and p_{old} have the same optimal basis.

Applying the theorem above, after computing the optimal solution for one pixel p of the image, we search the neighborhood of p to collect pixels that have colors that lie within the bounds given by the theorem and for which we can use a matrix-vector multiplication to compute the optimal solution. Instead of solving a linear system to find x = B^{-1}y for each case, we precompute all ${}_{19}C_{15} = 3876$ matrix inverses for this problem (this includes slack and surplus variables) and ignore row permutation costs during processing. This reduces the complexity of finding x from $O(n^3)$ to $O(n^2)$ complexity, potentially a significant savings when processing video or large images.

3.1.3 Processing Connected Regions with Low Costs

As discussed in section 3.1.2, after computing the optimal solution for one pixel p we should search around it to collect as many pixels as possible which satisfy the condition specified by Theorem 3.1.1. There are several different methods to implement this search-and-collect procedure. Before we discuss those methods, it is necessary to briefly introduce the *bitmap*(*.bmp*) files, which are used in our problem to store images. Bitmap is a standard file format used by Microsoft Windows. Bitmap files use the RGB color system to encode color at each pixel, and store color information of all pixels as a 2D array in row-major order. In other words, the red, green, and blue values of a pixel at the i_{th} row and j_{th} column of a $m \times n$ image are stored at the $[(i-1) \times n + j]_{th}$ position in the data region of the .bmp file. Although there are other popular file formats which do not record color for each pixel and are more space-efficient, we use .bmp files in our problem because they contains the RGB color coordinates which eliminates the overhead of having to derive them..

In accordance with the .bmp files, pixels of an image are processed in the row-

major order. In other words, an image is scanned from the bottom row to the top row, and from the left to the right within each row. Our first method is a simple search which follows this scanning mechanism naturally. It investigates pixels following p in the same row, where p is the pixel for which we have an optimal solution. We implemented this method by maintaining a matrix B to be the optimal basis of the last pixel we processed. Every time before processing a pixel q, we use the matrix B to check whether q satisfies the condition specified by Theorem 3.1.1, and process q with low cost if it does. If q doesn't satisfy the condition, it is processed by solving the associated LP, and the optimal basis of q becomes the new B matrix. This simple search reduces the running time of the program by 55 to 65 percent on our uniprocessor system for the set of continuous tone images we chose.

In view of the analysis in section 3.1.1, after computing the optimal solution for a pixel p, we would like to search around p and collect the entire connected region of pixels with colors close to p's. A simple row search does not accomplish this task. Therefore we extend the procedure to include a depth-first search starting from pixel p. Depth-first search is an algorithm for traversing a graph[15]. We implement the depth-first search with a stack technique, as described with pseudo-code in Algorithm 1:

```
Input: pixel p, for which the optimal solution has been computed
Result: collect the connected region surrounding p satisfying the condition
        specified by Theorem 3.1.1
build stack S;
mark p as processed;
push p into S;
while s not empty do
    t ← top of S;
    process t with matrix-vector multiplication;
    pop t;
    for i ← 1 to 8 do
        t_i ← i_th neighbor of t;
        if t_i and p satisfy the condition specified by Theorem 3.1.1, and t_i is
        not marked as processed then
            push t_i into S;
            mark t_i as processed;
        end
    end
end
```

Algorithm 1: Depth first search around pixel p

The procedure described in Algorithm 1 collects the entire connected region surrounding p satisfying the condition specified in Theorem 3.1.1. To see this point we use a counter-proof technique. Assume the point is not true, i.e., there is a pixel q in the connected region that is never visited in the depth-first search. From our definition of connected regions in section 3.1.1 we know that there exist pixels $q_1, q_2 \dots q_m$, all of which satisfy the condition specified by Theorem 3.1.1. Moreover, q_1 is a neighbor of p, q_i is a neighbor of q_{i+1} for $i = 1, 2, \dots, m-1$, and q_m is a neighbor of q. We assume q is never visited, so q_m never enters stack S either, because otherwise when q_m exits S q is pushed into S. Use the same argument we can conclude that none of $q_{m-1}, q_{m-2} \dots, q_1$ is visited by the search, which is impossible because when p exits S, q_1 is pushed into S as p's neighbor.

Based on the depth-first search algorithm above, we develop the method to process the entire image. Initially all pixels are marked as *unprocessed*. Then the image is still traversed in row-major order. But when we meet a pixel marked as *processed*, we do not try

execute the simplex algorithm to solve the associated LP because we know it has already been processed with matrix-vector multiplication. The procedure is described in Algorithm 2:

```
Input: image Im
Result: process Im with the d-f search acceleration technique
mark each pixel of Im as unprocessed;
h ← height of Im;
w ← width of Im;
for i ← 1 to h do
    for j ← 1 to w do
        p ← the (i, j)_th pixel of Im;
        if p is marked as unprocessed then
            execute the simplex algorithm to get the optimal solution for p;
            call the function defined in Algorithm 1 with input p ;
        end
    end
end
```

Algorithm 2: Algorithm for processing the entire image

From Algorithm 2 we can observe that when the program runs, the number of times that the simplex algorithm is executed can be no larger than $i \times w$. With this observation, we can see how the acceleration mechanism works on the images of Figure 3.3([1]). Figure 3.3(c) is the rendered stereo image, while Figures 3.3(a) and 3.3(b) are partially completed results of the program with variable i incremented to $\frac{h}{5}$ and $\frac{h}{2}$, respectively. In Figure 3.3(a) and 3.3(b), pixels in gray areas are not processed yet, or in *unprocessed* status, and pixels with the same color as in Figure 3.3(c) are in *complete* status. In Figure 3.3(c) we can see several connected regions with similar colors, such as the sky and many parts of the man's clothes. Figures 3.3(a) and 3.3(b) illustrates how these regions are processed with low cost. In Figure 3.3(a), $i = \frac{h}{5}$, which means the simplex algorithm is executed no more $\frac{h \times w}{5}$ times. But it is obvious that besides pixels in the lowest fifth of the image, many others have already processed, including pixels in the left part of the sky region. In Figure 3.3(b) the simplex algorithm is executed no more than $\frac{h \times w}{2}$ times, but most of the image has been processed. To conclude, as the program runs, the number of pixels processed is obviously larger than the number of times that the simplex algorithm is executed. In other words, a

(a) $i = \frac{h}{5}$ (b) $i = \frac{h}{2}$ (c) Complete image

Figure 3.3: Depth-first searching mechanism

considerable number of pixels are processed with matrix-vector multiplications, which have lower costs.

3.2 Parallel Processing

3.2.1 Parallelization without Color Coherence

The increase in speed of the UN calculation described above is not sufficient to render images of size 1K by 1K at video rates on our uniprocessor system. Hence we sought to apply parallel processing techniques to further reduce the total running time.

There are obvious parallel computation techniques that can be applied to our problem that do not require an elaborate connection network and message passing. See Foley, van Dam, Feiner and Hughes[6] for an overview of parallel rasterization methods. A natural approach is to divide the image into several equal parts and pass each part to a different processor. If we do not include the depth-first search, computations for nonintersecting parts can be treated as completely independent; all pixels are processed independently. Thus we can expect that the processing speed will grow linearly with the number of processors. This point is verified by our experimental data shown in section 4.2.

We design a message-passing program with C++ and MPI to implement the parallel computation. In accordance with the row-major order introduced in section 3.1.3, each processor is assigned an equal number of consecutive rows. For reasons that we will see in section 3.2.2, each processor reads the entire image; only the responsibilities of processing different parts of the image are divided among processors. This strategy does not have an observable impact on the performance of the program. When all processors finish processing

their assigned parts, they send their results to a *root* processer which is selected randomly. The root then creates the UN anaglyph image from all the processed pixels it receives.

3.2.2 Parallelization and Color Coherence

The analysis of the parallel computation becomes much more complex if the depth-first search acceleration technique discussed in section 3.1.3 is included. Even for a given image we expect that different data dividing schemes can result in considerably different performance.

In section 3.1.3 we have verified that in the uniprocessor case, after computing the optimal solution for a pixel p the depth-first search collects the entire connected region surrounding p and having colors close to p's. However, for a certain processor $proc_i$ in the parallel computation environment, the depth-first search can only collect pixels assigned to $proc_i$. In other words, the depth-first search can not go across partition boundaries. In the uniprocessor case, for one connected region r containing pixels with coherent colors, the simplex algorithm just needs to be executed once. In the parallel computation, if r is divided among m processors, then the simplex algorithm needs to be executed m times.

Here we show an extreme example. Consider the image in Figure 3.4(a) where all pixels in a column have the same color; for each column, the program has to execute the expensive simplex algorithm calculation once. If we use the row-wise dividing scheme, each processor is assigned a set of consecutive rows of the image, as in Figure 3.4(b), and the color coherence cannot be fully exploited. However, applying the column-wise method to divide the image, as in Figure 3.4(c), all the pixels in the column are processed at low cost. If we divide the image into nearly square blocks, each processor gets a block as shown in Figure 3.4(d), and we expect the execution time to lie between that of the other two methods (assuming, of course, processors of equal power).

It is a challenging problem to preserve color coherence when dividing data among processors. We are trying many methods to solve this problem. One prospective solution is first preprocessing the image to recognize its major connected regions with coherent colors, and then trying to assign each region to a single processor. Another method is to enable each processor to mark any pixel as *processed*, no matter if the pixel is assigned to this processor or not. If a depth-first search of $proc_i$ tries to collect a pixel p_j which is assigned to processor $proc_j$, it can do so after marking p_j as *processed* in both $proc_i$ and $proc_j$'s

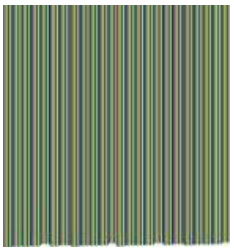

(a) Original image

(b) Row-wise dividing

(c) Column-wise dividing

(d) Block-wise dividing

Figure 3.4: An extreme example

memory. Thus $proc_j$ will not try to process p_j again. The methods discussed above is still in the progress of being developed, and there still remain many interesting problems.

3.2.3 Load Balancing

Load balancing is an important issue in parallel computing, and also in our particular problem. Obviously, there is no static data dividing scheme that is best for all images. We expect some processors to require more computation than others, because our algorithm takes advantage of color coherence which can be very irregular. To show this we apply our UN algorithm on several pairs of continuous tone images, with different numbers of processors and different data dividing schemes. As expected, we found that there is considerable difference between the running times of different computing nodes. We also notice a trend that the imbalance can grow with the number of processors applied to the problem. Since we are interested in processing video data, we seek a predistributed load balancing scheme that monitors processor computing requirements over successive frames and adjusts partitioning accordingly.

To study the problem we first develop a partition adjustment algorithm where workloads for different nodes on a static image are modified. We first run the parallel

algorithm with static data dividing scheme, sort the execution times for each processor and then reallocate to attempt to attain the optimal allocation where each processor requires the same amount of execution time(if such an allocation exists). The reallocation algorithm is discussed in section 4. Our experiments show that this can reduce processing time considerably. We are trying to extend this partitioning adjustment method for processing video.

Another focus of our future work will be to develop a method for processor communication so that workload can be adjusted during calculation on a single frame. In a message passing scheme there are many challenges, such as how to reduce communication cost and how to transmit workload among a large number of processors. In the following section we present our computation results.

Chapter 4

Acceleration Results

4.1 Results of Exploiting Color Coherence

We discuss the effects of exploiting color coherence. The experiments are performed on a Dell 700m laptop computer with Intel Pentium M 1.6GHz processor and 512MB memory. Three different implementations of the UN calculation are tested: the original program where **no search** is performed and colors of all pixels are computed using the simplex algorithm, the program with **simple search** along the row of the calculated pixel and the program with **depth-first search (D-F search)** around the calculated pixel, as described in section 3.1. To illustrate the effect of exploiting color coherence on different images we chose a set of image pairs with different sizes and features as shown in Figure 4.1 from Johnson and McAllister[8], Figure 4.2 from Hannisian[7] and Figure 4.3 from our website[1]. The stereo images rendered with UN method are also displayed in the figures. Larger views of the images are given in Appendix B. The running times for processing these images are listed in Table 4.1.In all tables in this section and section 4.2, running times are measured in seconds.

Simple search reduces the running time by 52 to 77 percent. The depth-first search further reduces the running time by 33 to 53 percent for a total speedup percentage of 72 to 89 percent. For images with relatively complicated color patterns and strong color contrasts as Figure 4.2, the speedup from exploiting color coherence is not as pronounced as that for

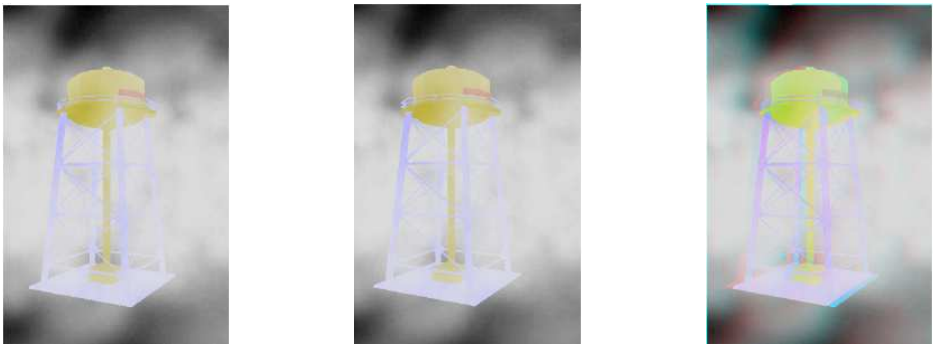

(a) Left eye view (b) Right eye view (c) Stereo image

Figure 4.1: A 203×305 pair of images

(a) Left eye view (b) Right eye view (c) Stereo image

Figure 4.2: A 230×261 pair of images

(a) Left eye view (b) Right eye view (c) Stereo image

Figure 4.3: A 1085×675 pair of images

Table 4.1: The result of exploiting color coherence with different searching mechanisms

	Size	**No Search**	**Simple Search**	**D-F Search**
Figure 4.1	203×305	11.02	2.51	1.19
Figure 4.2	230×261	9.98	4.82	2.80
Figure 4.3	1085×675	127.54	45.55	30.45

images with relatively simple patterns and weak color contrasts as Figure 4.1.

4.2 Results of Parallel Computing

In this section we will discuss the effect of applying parallel processing techniques to reduce the total running time. The experimental test bed is NCSU's IBM Blade Center Linux Cluster Henry2, with up to 16 computing nodes with 2.8-3.06 GHz Intel Xeon Processors and 4GB per node distributed memory. Our experiments are performed on the pairs of images in Figure 4.3 in section 4.1. In a parallel environment, running time is the time required by the longest running processor.

First we ran the original program (all pixels are processed with the simplex algorithm) on an increasing number of processors to determine how the running time and computing speed (reciprocal of running time) of the program vary with the number of processors. From Table 4.2 we can see that, as expected, there is an approximately linear speedup with the number of processors. Since there is no interprocessor communication or search, the speedup will be approximately linear regardless of the number of processors. The running time on one node is 103 seconds vs. the 127 seconds on the uniprocessor system because in this case, each node of the cluster has a much faster processor (2.8-3.6 GHz) than that of the uniprocessor we use in section 4.1 (1.6 GHz).

Table 4.2: The running time varying with the number of computing nodes

Number of nodes	1	2	4	8	16
Running time	103	56	27	16	10

Our next experiment was to run the program with a depth-first search on varying number of processors and different data dividing schemes. Row-wise, column-wise and block-wise data dividing schemes are applied, as described in section 3.2. Table 4.3 lists

the result for each combination of number of processors and data dividing schemes. In the table, **Rows** $\times$ **Columns** defines how the image is divided among the computing nodes. For example, if the entry is 4×2, the image is divided by $8 = 4 \times 2$ processors into a 4 by 2 array. In the vertical dimension the image is divided into 4 equal parts and in the horizontal dimension it is divided into two.

Table 4.3: Shortest and longest running times with different data dividing schemes

Rows $\times$ *Columns*	Shortest running time	Longest running time
2×1	12.48	19.23
1×2	12.29	16.78
4×1	4.20	9.32
2×2	6.26	9.37
1×4	6.56	8.81
8×1	1.59	5.68
4×2	1.65	6.18
2×4	2.57	4.81
1×8	2.96	4.84

The imbalance among the workloads of different processors is obvious and it grows with the total number of processors. The largest relative difference occurs at 4×2, where the longest running time is 3.7 times the shortest. Also note the difference between the 4×2 and the 2×4 cases which we would hope to be approximately the same. It is also clear that imbalance exists for all the three dividing schemes described in section 3.2: row-wise, column-wise and block-wise. Considering the irregular patterns of images to process, we can further conclude that no static data dividing scheme will achieve balanced workloads among all processors.

We experiment with the static balancing algorithm introduced in section 3.2, where we sort running times of processors and repartition the workload to attempt to achieve uniform running times. We have tested the program on the images in Figure 4.3 with two processors, the 2×1 case above. First we partition the image equally where the lower and upper parts are assigned 337 and 338 rows of the images, respectively. In this case the running times are 19.23 seconds for the lower part and 12.48 seconds for the upper, a wide variation.

We then apply a simple algorithm that computes an adjustment according to the relative difference of the running times, i.e., taking half of the difference between the

running times, computing its percentage in the total runtime and adjusting the number of rows accordingly. In this case the adjustment would be $\frac{19.23-12.48}{2} \times \frac{675}{19.23+12.48} = 60.4$, so the modified workload of the lower part should be 337 - 60 = 277 rows and the workload of the upper part should be 398 rows. However, as shown in the second part of Table 4.4 below, there is still imbalance between the running times of the two processors; because of the idiosyncrasies of this particular image the upper part has a longer running time, which means we have over-adjusted the workloads. Thus, we try cutting the adjustment by half, i.e., from 60 rows to 30 rows. The result is shown in the third part of Table 4.4. We can see that although the upper part still has a longer running time, the imbalance is less. A similar approach can be formulated for more than 2 processors.

Table 4.4: Results of different workload distributing schemes

	Range of rows computed	Running time
Upper part	338 to 675	12.48
Lower part	0 to 337	19.23
Upper part	278 to 475	15.45
Lower part	0 to 277	13.14
Upper part	308 to 675	13.90
Lower part	0 to 307	13.52

By applying the static balancing approach we improve the performance from 19.23 seconds to 15.45 seconds in the first case, and to 13.90 seconds in the second case. Moreover, from the above table we can see the trend that if we keep modifying the adjustment according to the difference in running times, the dividing scheme will eventually converge to a balanced one where each processor has an approximately equal workload. This suggests that predistributed load balancing may be effective in processing video streams if we adjust the workload for a frame based on the processor running times for the previous frames.

4.3 Conclusion

In this section we list the results of several techniques to accelerate the UN anaglyph calculation. It is clear that our efforts were successful in reducing the time for rendering an anaglyph image using the UN algorithm. For the case of the 1085×675 image in Figure 4.3, the total processing time is reduce from 127 seconds (on 1 processor, be-

fore taking advantage of color coherence) to 4.84 seconds (on 8 processors, exploiting color coherence with depth-first search).

Chapter 5

Conclusion and Future Direction

We have described how to use UN approximation and the implied linear programming to solve an anaglyph computation problem. We compared the results with other methods to compute anaglyphs and concluded that there is still considerable work to be done.

Our future research will be focused on real time video rendering, with the challenge of exploiting the coherence between adjacent video frames and achieving a balanced workload among processors.

We also intend to examine approximation in uniform color spaces such as CIEL*a*b* and consider developing image processing filters to adjust images to reduce ghosting. Additionally, we are considering methods to modify algorithms so that solutions have the equal color preservation property.

Bibliography

[1] *Anaglyph stereo images.* NCSU Computer Science Department Research in Stereo Computer Graphics, http://research.csc.ncsu.edu/stereographics/.

[2] Dimitris Bertsimas and John N. Tsitsiklis. *Introduction to Linear Optimization.* Athena Scientific, Nashua, NH, 1997.

[3] Randy Crane. A simplified approach to image processing. Upper Saddle River, NJ, 1997. Prentice Hall PTR.

[4] Keely L. Croxton. *Graph about simplex algorithm, http://fisher.osu.edu/˜croxton_4/tutorial/Geometry/simplex.html.*

[5] Eric Dubois. A projection method to generate anaglyph stereo images. volume 3 of *Proc. IEEE Int. Conf. Acoustics Speech Signal Processing*, pages 1661–1664, Salt Lake City, UT, 2001. IEEE.

[6] J. D. Foley, A. van Dam, S. K. Feiner, and J. F. Hughes. *Computer Graphics: Principles and Practice.* Addison-Wesley Professional, 1995.

[7] Ray Hannisian. Los huicholes. *stereo image on http://www.ray3d.com/road.html/.*

[8] Tyler Johnson and David F. McAllister. Realtime stereo imaging of gaseous phenomena. volume 5664 of *Proc. SPIE*, pages 92–103, 2005.

[9] B. Julesz. *Foundations of Cyclopean Perception.* University of Chicago Press, Chicago, IL, 1971.

[10] N. Karmarkar. A new polynomial-time algorithm for linear programming. volume 4 of *Combinatorica*, page 373C395, 1984.

[11] D. F. McAllister. *Stereo Computer Graphics and other True 3D Technologies*. Princeton U. Press, Princeton, NJ, 1993.

[12] D. F. McAllister. *3D Displays*. Wiley Encyclopedia on Imaging, 2002.

[13] D. F. McAllister and Preshant D. Hebbar. Color quantization aspects in stereopsis. volume 1457 of *SPIE Proceedings Stereoscopic Displays and Applications II*, pages 233–241, Bellingham,WA, 1991. SPIE.

[14] W. Sanders and David F. McAllister. Producing anaglyphs from synthetic images. volume 5006 of *Proc. SPIE*, pages 348–358, 2003.

[15] R.E. Tarjan. Depth-first search and linear graph algorithms. volume 1 of *SIAM J. Comput*, pages 146–160, 1972.

[16] C. Wheatstone. Contributions to the physiology of vision-part the first. on some remarkable and hitherto unobserved phenomena of binocular vision. volume 128 of *Philos Trans R Soc Lond*, pages 94–371, 1838.

[17] Andrew J. Woods and John Merritt. Stereoscopic display application issues. *SPIE Electronic Imaging (Short Course)*, 2002.

[18] Andrew J. Woods and Tegan Rourke. Ghosting in anaglyphic stereoscopic images. volume 5291 of *Proc. SPIE*, 2004.

Appendix A

Color Comparison Results

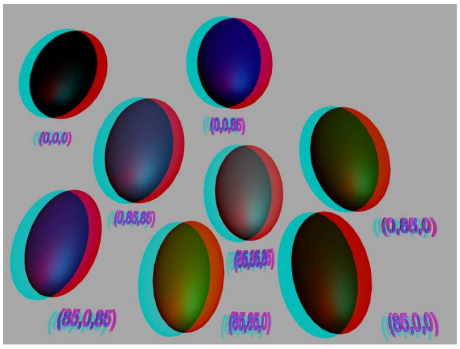

(a) LS

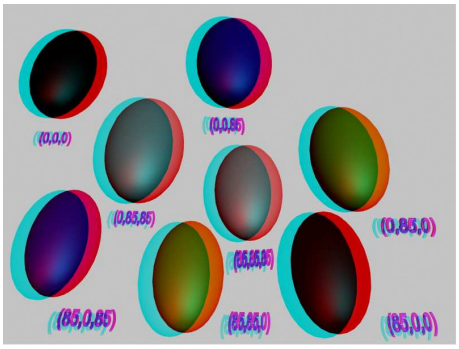

(b) MPS

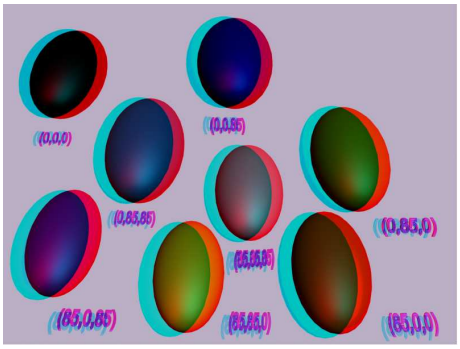

(c) UN

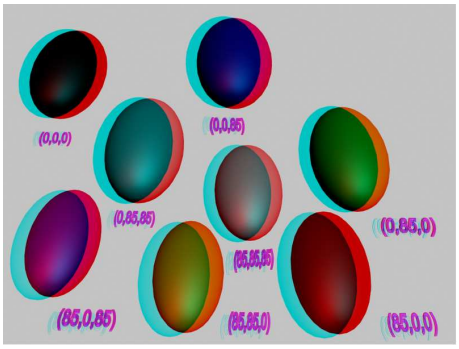

(d) PS

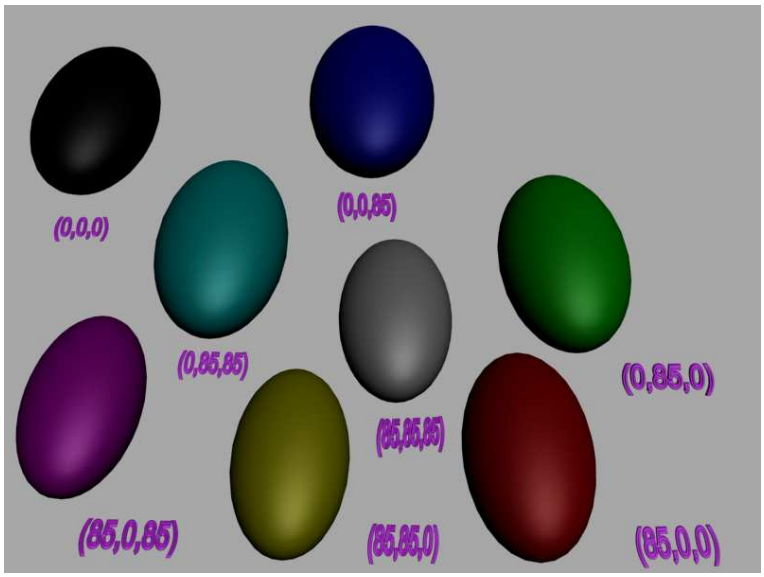

(e) Left eye view with true color

Figure A.1: Cube 1 - Stereo image rendered with different methods

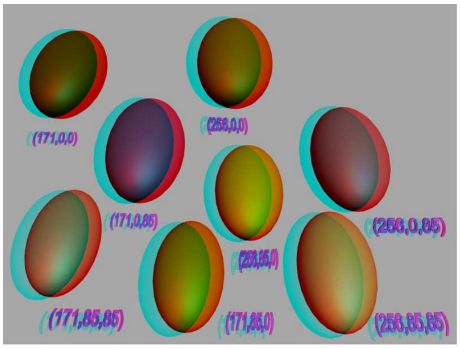

(a) LS

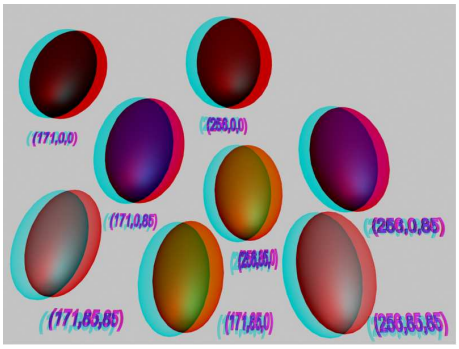

(b) MPS

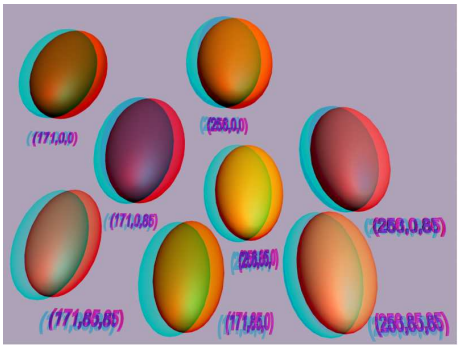

(c) UN

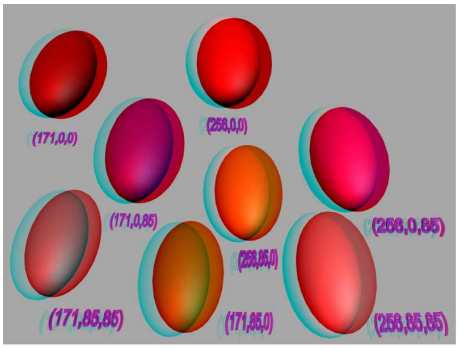

(d) PS

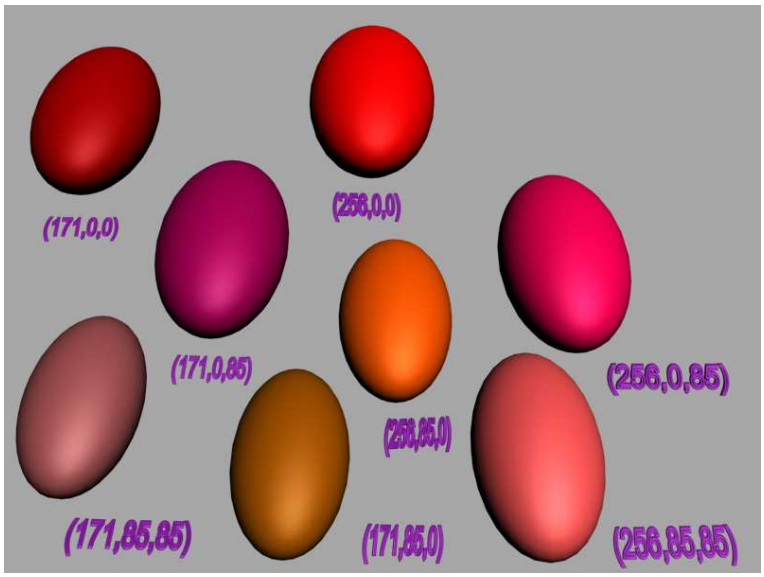

(e) Left eye view with true color

Figure A.2: Cube 2 - Stereo image rendered with different methods

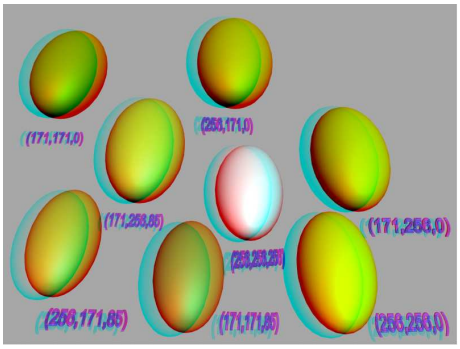

(a) LS

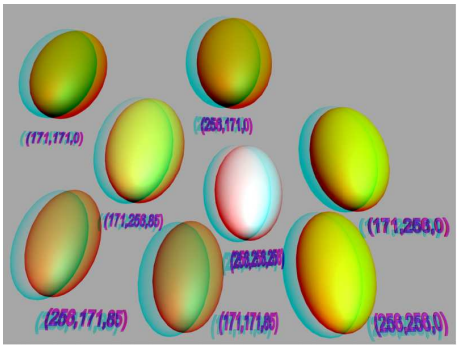

(b) MPS

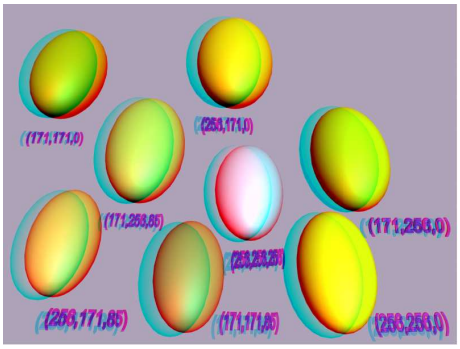

(c) UN

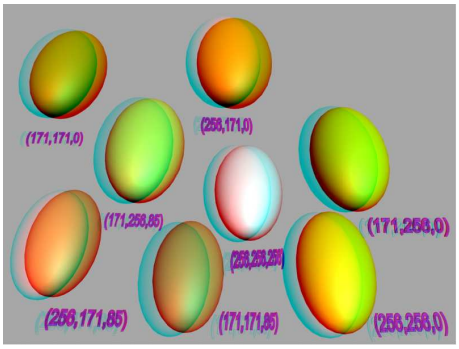

(d) PS

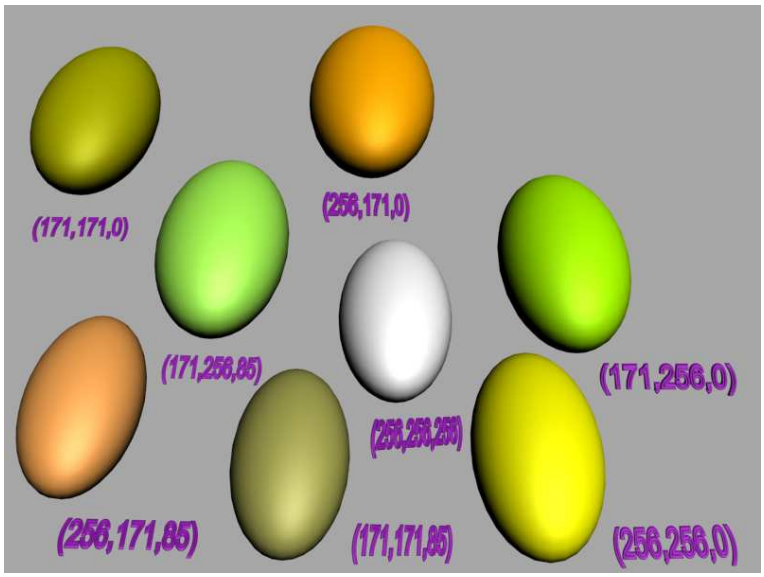

(e) Left eye view with true color

Figure A.3: Cube 3 - Stereo image rendered with different methods

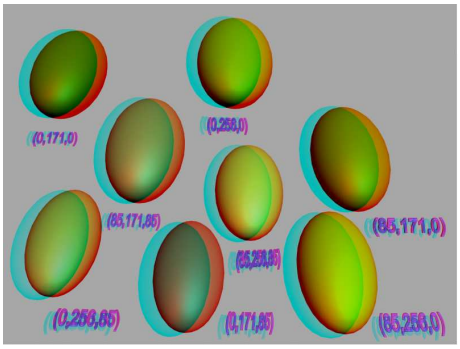

(a) LS

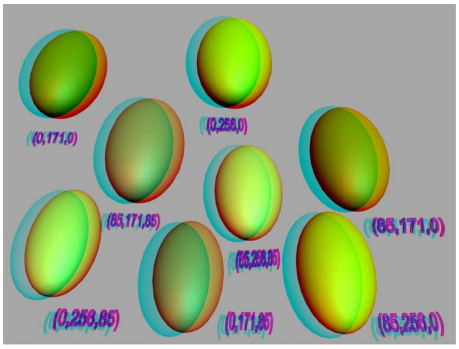

(b) MPS

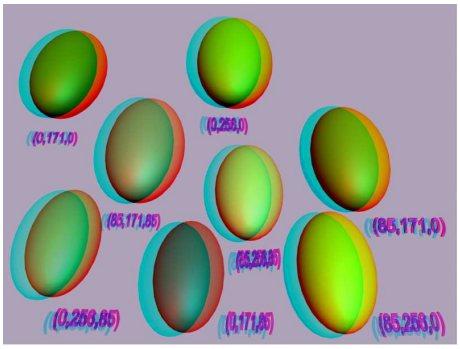

(c) UN

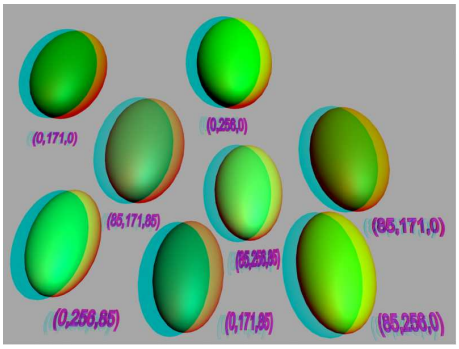

(d) PS

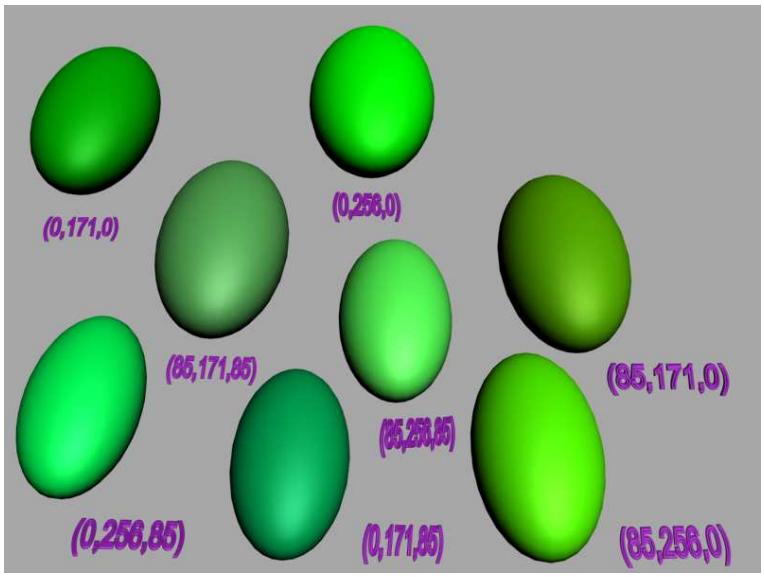

(e) Left eye view with true color

Figure A.4: Cube 4 - Stereo image rendered with different methods

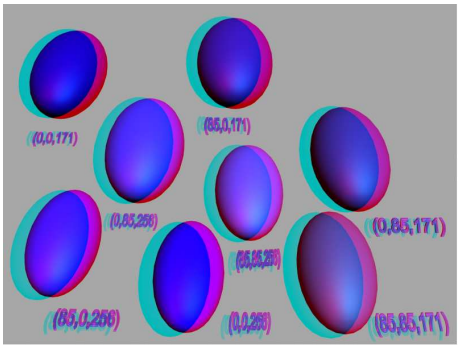

(a) LS

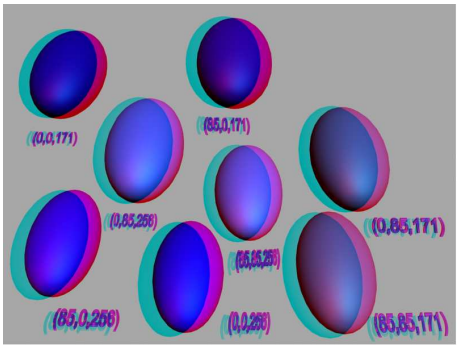

(b) MPS

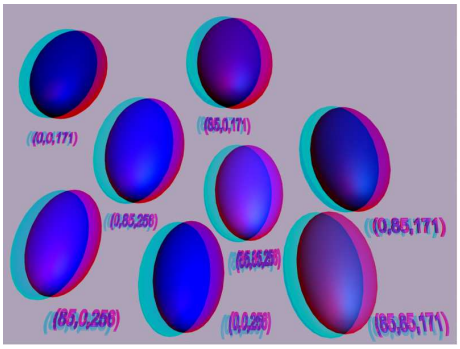

(c) UN

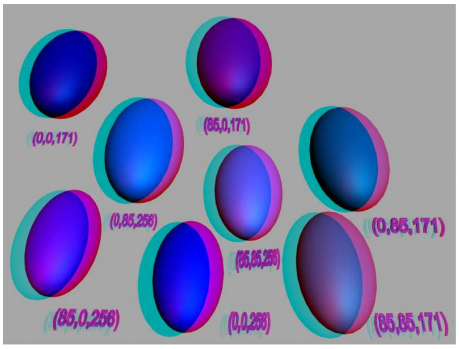

(d) PS

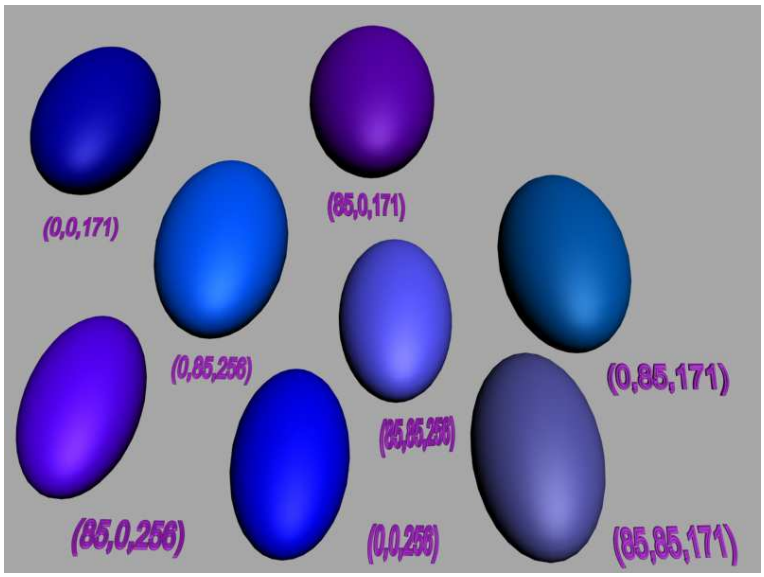

(e) Left eye view with true color

Figure A.5: Cube 5 - Stereo image rendered with different methods

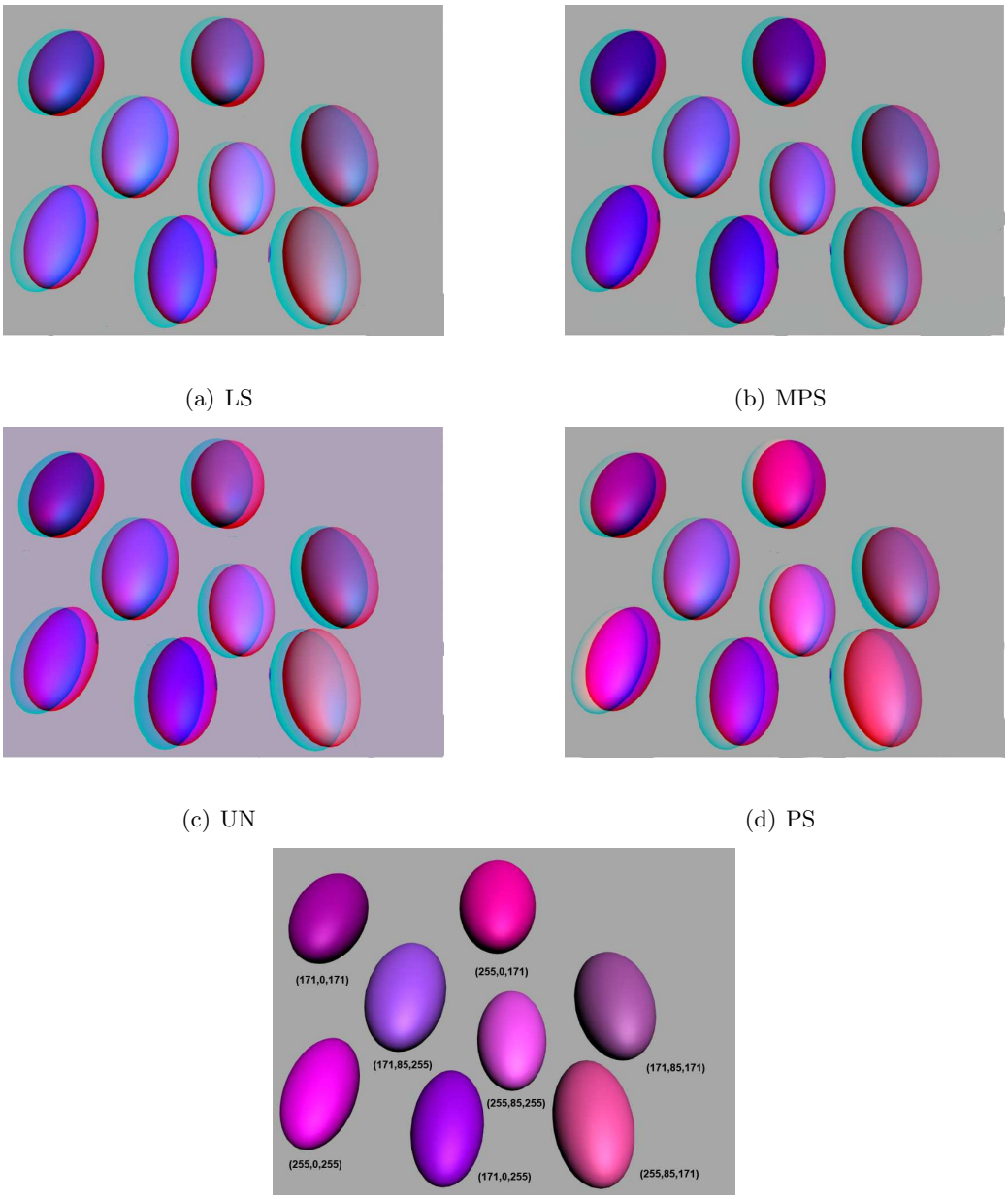

(a) LS

(b) MPS

(c) UN

(d) PS

(e) Left eye view with true color

Figure A.6: Cube 6 - Stereo image rendered with different methods

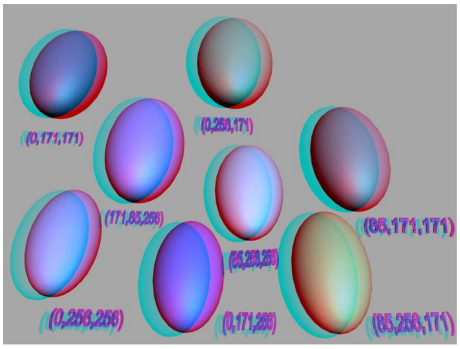

(a) LS

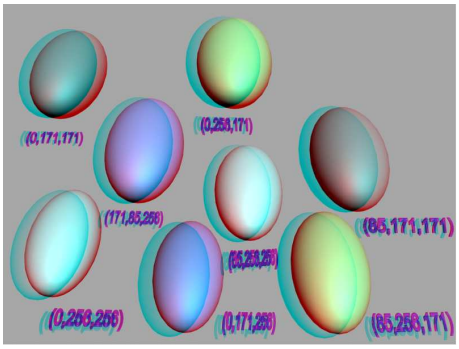

(b) MPS

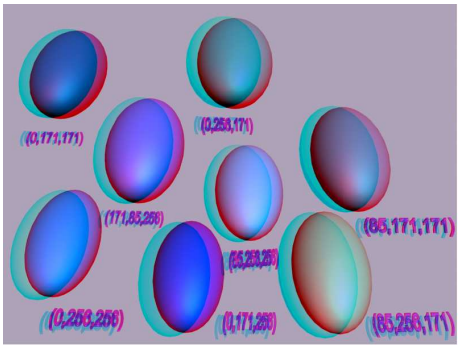

(c) UN

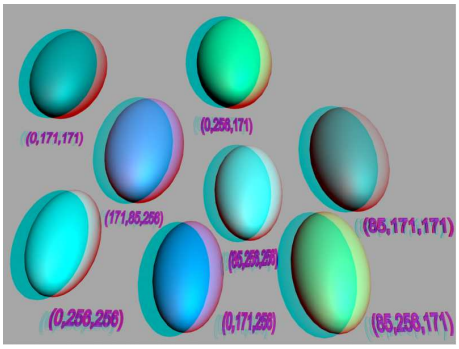

(d) PS

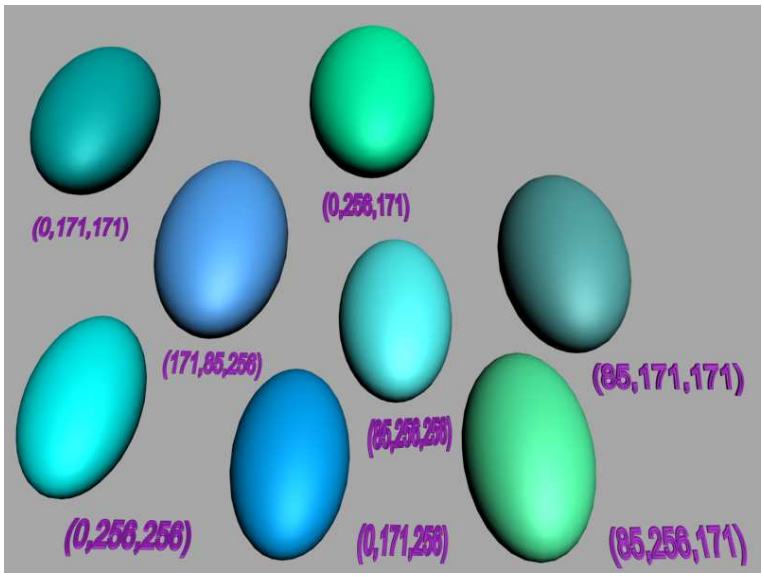

(e) Left eye view with true color

Figure A.7: Cube 7 - Stereo image rendered with different methods

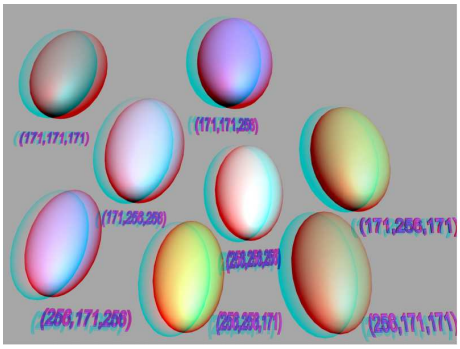

(a) LS

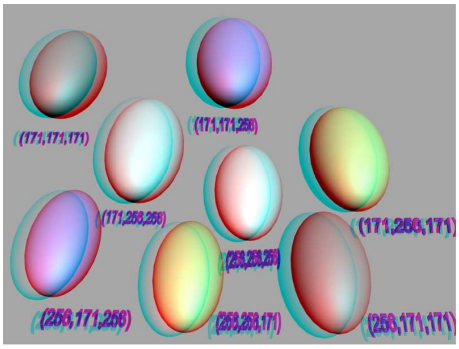

(b) MPS

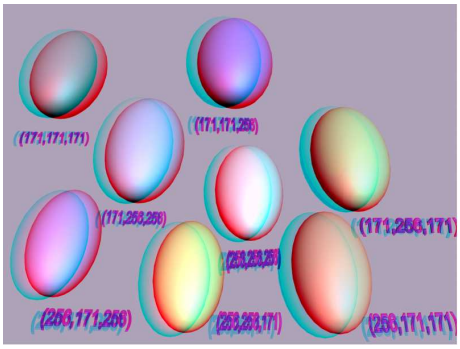

(c) UN

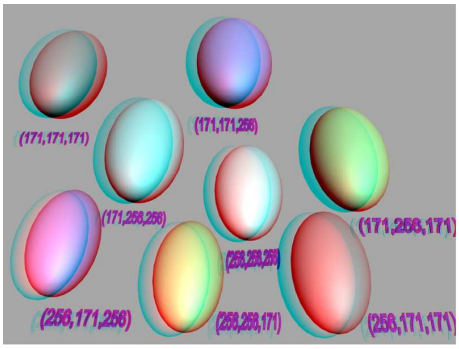

(d) PS

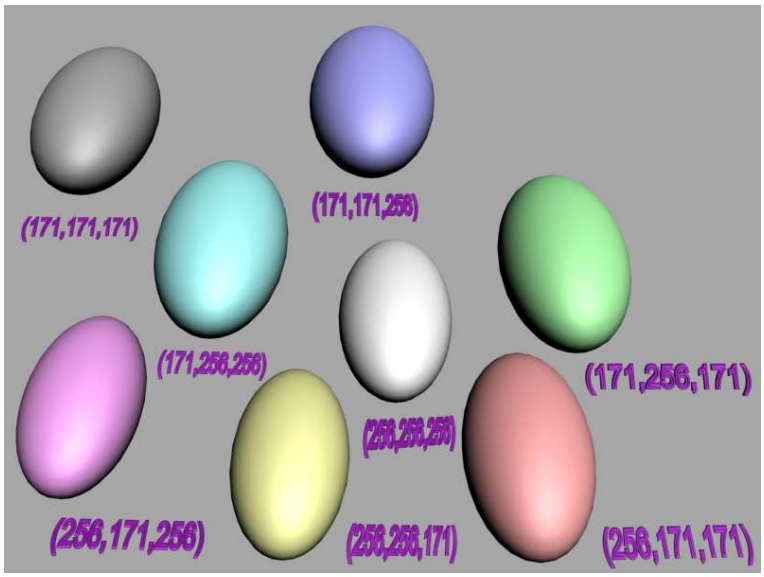

(e) Left eye view with true color

Figure A.8: Cube 8 - Stereo image rendered with different methods

Appendix B

Acceleration Results

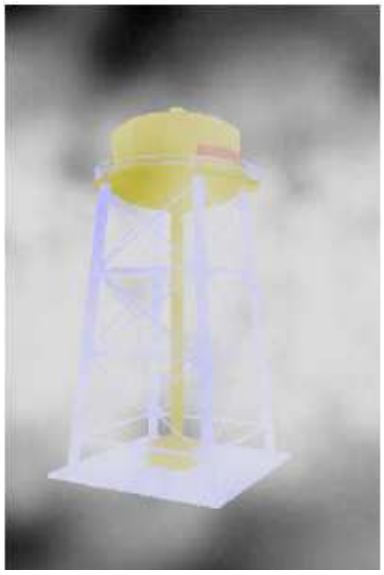

(a) Left eye view

(b) Right eye view

(c) Stereo image

Figure B.1: A 203×305 pair of images

(a) Left eye view

(b) Right eye view

(c) Stereo image

Figure B.2: A 230×261 pair of images

(a) Left eye view

(b) Right eye view

(c) Stereo image

Figure B.3: A 1085×675 pair of images